Transient proliferation by reversible YAP and mitogen-control of the cyclin D1/p27 ratio

Katherine R. Ferrick[1,2], Yilin Fan[1,2,3], Nalin Ratnayeke[1,2,4], Mary N. Teruel[5], Tobias Meyer[1,2,6,*]

[1]Department of Cell and Developmental Biology, Weill Cornell Medicine, New York, NY, USA
[2]Department of Chemical and Systems Biology, Stanford Medicine, Stanford, CA, USA
[3]Current: Department of Pathology and Center for Cancer Research, Massachusetts General Hospital and Harvard Medical School, Boston, MA, USA
[4]Current: Cancer Biology and Genetics Program, Sloan Kettering Institute, Memorial Sloan Kettering Cancer Center, New York, NY, USA
[5]Department of Biochemistry, Weill Cornell Medicine, New York, NY, USA
[6]Lead contact
[*]Correspondence: tom4003@med.cornell.edu

ABSTRACT

Hippo-YAP signaling orchestrates epithelial tissue repair and is therefore an attractive target in regenerative medicine. Yet it is unresolved how YAP integrates with mitogen signaling and contact inhibition to control the underlying transient proliferative response. Here we show that reduced contact inhibition, increased mitogen signaling, and YAP-TEAD activation converge on increasing the nuclear cyclin D1/p27 protein ratio during G1 phase, towards a threshold ratio that dictates whether individual cells enter or exit the cell cycle. YAP increases this ratio indirectly, in concert with mitogen signaling, by increasing EGFR and other receptors that signal primarily through ERK. After a delay, contact inhibition suppresses YAP activity which gradually downregulates mitogen signaling and the cyclin D1/p27 ratio. Increasing YAP activity by ablating the suppressor Merlin/NF2 reveals a balancing mechanism in which YAP suppression and contact inhibition of proliferation can be recovered but only at higher local cell density. Thus, critical for tissue repair, robust proliferation responses result from the YAP-induced and receptor-mediated prolonged increase in the cyclin D1/p27 ratio, which is only reversed by delayed suppression of receptor signaling after contact inhibition of YAP.

INTRODUCTION

Acute chemical and physical injuries inactivate the Hippo pathway, resulting in transient activation of the transcriptional cofactor YAP to increase proliferation, induce metabolic changes, and promote matrix remodeling[1,2]. YAP activation and nuclear translocation initiates transcription through binding to TEAD and other nuclear transcription factors[3]. Though YAP and its paralog TAZ are dispensable for the basal proliferation of several tissues, they are crucial for regeneration and repair following injury in tissues such as skin, liver, and kidney[1]. Inhibitors of Hippo pathway proteins are therefore being developed for potential clinical use in tissue repair[4–6]. While the core genes regulating the Hippo pathway are well-established, the complexity of the downstream signaling processes has made it difficult to resolve the molecular mechanism of the transient proliferation response using animal models.

Hippo signaling is kept active in epithelial sheets and other tissues by cell-cell contacts, such as adherens and tight junctions, and is inactivated by mechanical stress during tissue repair[1,7,8]. Adaptor proteins like Merlin (NF2) contribute to contact inhibition signaling to activate LATS1/2, which is the principal kinase of the Hippo pathway suppressing YAP-TEAD activity through multisite phosphorylation[9,10]. Consequently, loss of Merlin or LATS activity leads to

49 dramatic increases in the size of tissues and organs, and tumorigenesis[9,11,12]. Despite the
50 general role of YAP activation in promoting proliferation, the mechanism by which YAP
51 integrates with other signaling pathways to regulate both cell cycle entry and exit is unresolved.
52 Different mechanisms have been described through which YAP signaling could increase
53 proliferation. Constitutive YAP activation increases expression of a broad array of cell cycle
54 genes, including DNA replication factors and regulators of G2/M progression[13–15]. YAP also
55 promotes secretion of various signaling regulators[16,17]. However, cell cycle entry is not only
56 controlled by YAP, but is also regulated by both receptor signaling and contact inhibition[18,19].
57 Ultimately, cell cycle entry is controlled by cyclin-dependent kinase (CDK) activation in G1
58 phase which must phosphorylate and inactivate retinoblastoma protein (Rb), the suppressor of
59 the cell cycle transcription factor E2F. As persistent YAP activation induces organ hyperplasia
60 and cancer, YAP-TEAD must be robustly inactivated after its initial induction, once the tissue
61 repair is completed. Thus, to understand tissue repair, it is crucial to determine how YAP,
62 mitogens, and contact inhibition control Rb phosphorylation to first promote and then suppress
63 cell cycle entry.
64 Here we use multiplexed, single-cell immunofluorescence analysis to examine YAP-
65 regulated proliferation in thousands of epithelial cells in a monolayer. We show that over a wide
66 range of stimuli, proliferation is controlled through a balance mechanism whereby mitogen
67 signaling is opposed by contact inhibition of YAP. Strikingly, mitogen signaling, contact
68 inhibition, and YAP-activation converge on the cyclin D1/p27 ratio during G1 phase, which
69 dictates whether Rb is phosphorylated and cells enter the cell cycle. We show that YAP
70 activation increases the levels of EGFR and other surface receptors, which in turn signal
71 primarily through MEK-ERK to increase the cyclin D1/p27 ratio. We further identify the
72 mechanism that prolongs the proliferation response: acute inactivation of YAP gradually
73 reduces EGFR signaling to lower the cyclin D1/p27 ratio but only after a delay. Moreover, we
74 show that YAP signaling can be robustly terminated: even a strong increase in YAP activity
75 generated by ablation of the upstream Hippo component Merlin could still be reversed by
76 contact inhibition of YAP, but only at higher local cell density. Together, our study identifies a
77 YAP-controlled balancing mechanism between contact inhibition and receptor signaling that
78 drives an increase and delayed decrease in the cyclin D1/p27 ratio. The delay in the balance
79 ensures that the YAP-induced proliferation response is prolonged to allow for sufficient cell
80 divisions while the robust YAP inactivation ensures that the proliferation response is inherently
81 transient.
82

RESULTS

Contact inhibition of YAP opposes mitogen stimulation in a balance mechanism controlling cell proliferation

To assess mitogen and density-dependent changes in proliferation, we measured both phosphorylation of retinoblastoma protein (p-Rb, S807/811), which is a bimodal marker of cyclin-CDK activity[20] that is low in arrested cells and remains high in cycling cells from G1 through mitosis, and EdU incorporation into DNA, which occurs during DNA replication in S phase (Figure 1A, S1A). We determined how YAP activity changes the mitogen dependence of proliferation by stably expressing a doxycycline (DOX)-inducible, constitutively active YAP variant (5 regulatory serines mutated to alanine[21], CA-YAP) in hTERT-immortalized human retinal pigmented epithelial cells (RPE1), which reversibly arrest the cell cycle with serum starvation or contact inhibition[22]. As leaky expression of CA-YAP (without DOX induction) was sufficient to increase proliferation (at a similar expression level compared to the endogenous YAP, Figure S1B), we did not use DOX induction unless otherwise stated.

Using increasing concentrations of serum (fetal bovine), we found that mean levels of proliferation (by both p-Rb and EdU, Figure 1B) were consistently higher in CA-YAP relative to wild type (WT) cells at all mitogen levels and serum-independent, as previously reported[23]. However, even within epithelial monolayers plated at identical densities and subject to the same mitogen stimuli, there is considerable heterogeneity in cell cycle signaling[22,24,25]. We therefore used single-cell analysis to distinguish between various plausible mechanisms of how YAP activation might be linked to both contact inhibition and mitogen signaling to control cell cycle entry. We use the terms “contact inhibition” and “local cell density” interchangeably since the local cell density in monolayers closely predicts whether proliferation is suppressed in individual RPE1 cells[22]. We quantified local cell density by subdividing segmented nuclei for each image into a 10 x 10 grid (~75 x 75 μm) and counting the cells within each block (Figure 1C). Each cell was then assigned its local density based on the number of cells in its block (Figure S1C, see also Methods) and compared with the fraction of proliferating cells (Figure 1D).

In WT cells, the proportion of proliferating cells progressively decreased as local cell density increased for high and low serum levels, supporting that mitogen signaling and local contact inhibition oppose each other in regulating proliferation (Figure 1E, S1D). This conclusion was also supported by an alternative metric of local cell density based on the area of neighboring cell nuclei within a radius of similar scaling[22] (Figure S1E).

116 Strikingly, even with weak YAP expression, the cell density dependence of proliferation
117 was abolished in CA-YAP cells regardless of mitogen levels (Figure 1E), demonstrating that
118 contact inhibition of proliferation requires contact inhibition of YAP activity. Moreover, this
119 confirmed that CA-YAP cells retained mitogen sensitivity independent of contact inhibition since
120 increasing serum levels further increased the percentage of proliferating cells. Thus, the inverse
121 regulation between mitogens and cell density represents an intuitive balancing mechanism: the
122 inhibition of proliferation at a given cell density can be overcome by increasing mitogen
123 signaling, and the increase in proliferation after increasing mitogen signaling can be
124 antagonized once cell division has increased local cell density. However, persistent activation of
125 YAP breaks the balance and makes proliferation independent of cell density.
126 We next tested whether contact inhibition and mitogen signaling regulate endogenous
127 YAP activity. As the ratio of the nuclear to cytoplasmic (n/c) YAP and the absolute nuclear level
128 of YAP are both relative measures of YAP activity[26,27], we measured both parameters as a
129 function of local cell density (Figure 1F). At 0.1% serum, we observed the expected inhibition of
130 the YAP n/c ratio and nuclear levels at increasing local density. At 1% and 10% serum, the YAP
131 n/c ratio decreased at higher cell densities, but the nuclear level of YAP was higher than for low
132 serum conditions. We used this single-cell data to analyze the percentage of cells with
133 phosphorylated Rb as a function of the relative YAP activity. Unexpectedly, using both metrics,
134 increasing serum levels increased proliferation for cells with identical YAP levels (Figure 1G).
135 Thus, while YAP activation and mitogen stimuli synergistically increase proliferation, we find that
136 mitogens can also increase proliferation directly without increasing YAP levels or localization.
137 Finally, we determined how acute increases and decreases in YAP activity regulate Rb
138 phosphorylation. Using recently developed inhibitors, we inhibited YAP-TEAD signaling with a
139 pan-TEAD inhibitor[28], and activated endogenous YAP using a LATS1/2 inhibitor[5,29]. We
140 confirmed that TEAD inhibition promoted a strong cytoplasmic localization of endogenous YAP
141 while LATS inhibition triggered its nuclear enrichment (Figure 1H). TEAD inhibition greatly
142 reduced the fraction of proliferating cells for low but not for high serum stimuli, suggesting that
143 YAP-TEAD activity is particularly critical for inducing proliferation for low mitogen stimulation
144 conditions (Figure 1I, S1F). Conversely, LATS inhibition greatly boosted proliferation at low
145 serum stimuli and had a smaller relative effect at high serum stimuli due to the already high
146 percentage of proliferating cells (Figure S1G). Finally, this analysis revealed that high mitogens
147 can induce proliferation independently of YAP-TEAD activity since TEAD inhibition could
148 reverse the portion of proliferation induced by YAP but not a YAP-independent component of
149 mitogen-induced proliferation (Figure 1I, Figure S1H).

150 We conclude that contact inhibition of YAP activity and mitogen signaling compete to
151 respectively suppress or promote proliferation over a wide range of cell densities and mitogen
152 stimuli. However, this balance can be broken in two ways: by high mitogen stimuli inducing
153 proliferation in cells lacking YAP-TEAD activity and persistent activation of YAP abolishing
154 contact inhibition of proliferation.
155
156 **YAP-regulated cell cycle entry and exit is dictated by the cyclin D1/p27 threshold**
157 We next used the quantitative analysis of the balance between contact inhibition and mitogen
158 signaling to identify the mechanism of how YAP regulation controls cell-cycle entry and exit.
159 Cells enter the cell cycle during the G1 phase by activating cyclin-CDK complexes to
160 hyperphosphorylate Rb and derepress the E2F cell cycle transcription program[20]. In contrast, in
161 cells that exit the cell cycle or stay arrested, cyclin-CDKs stay inactive and Rb remains
162 dephosphorylated. In monolayers of RPE1 and other epithelial cells, this bimodal Rb
163 phosphorylation is thought to be primarily controlled by the CDK4/6 activator cyclin D1 and the
164 cyclin-CDK2/4/6 inhibitor p27[22], and cyclin D1 is generally thought to contribute to the YAP-
165 mediated proliferation regulation[3]. We included p27 in our analysis since both cyclin D1[30] and
166 p27 are key regulators of cell proliferation in vivo, with p27 deletion resulting in multi-organ
167 hyperplasia[31].
168 Using image-based cytometry and multiplexed immunofluorescence[32], we first
169 computationally gated for G1 cells by their diploid 2N DNA content and lack of incorporation of
170 EdU (Figure S2A). We then measured the levels of nuclear localized cyclin D1 and p27 and
171 whether Rb was phosphorylated in each G1-phase cell. Notably, p27 protein levels are often
172 used as a marker of non-proliferating cells, but we observed substantial heterogeneity in the
173 nuclear levels of both p27 and cyclin D1 across individual cells irrespective of Rb
174 phosphorylation (Figure S2B). Increasing the mitogen stimulus (from 0.1% to 10% serum)
175 resulted in the cell population shifting towards higher average cyclin D1 levels and lower
176 average p27 levels.
177 We next determined how local cell density and YAP activity regulate the cyclin D1 and
178 p27 levels. As local density increased, the median cyclin D1 level of WT cells gradually
179 decreased, while the median p27 level strongly increased (Figure 2A). This trend was opposite
180 to the effects of increasing serum, which both globally increased cyclin D1 levels and
181 suppressed the density-dependent increase in p27 protein. Markedly, the CA-YAP cells lost the
182 serum and density dependence of both, keeping the levels of cyclin D1 high and p27 low in G1

183 phase, arguing that YAP activity is not only upregulating the level of cyclin D1 but also
184 downregulating the level of p27 (Figure 2B).
185 Explaining why the level of cyclin D1 or p27 alone cannot predict whether Rb is
186 phosphorylated, only the level of cyclin D1 relative to p27 was tightly correlated with Rb
187 phosphorylation in individual cells (Figure S2C). Only cells with relatively more cyclin D1 than
188 p27 had Rb phosphorylated (Figure 2C-D). Thus, even for low mitogen levels, a small fraction of
189 cells had sufficiently high cyclin D1 and low p27 to have Rb phosphorylated. Conversely, at high
190 mitogen stimulation, more cells populated the high-cyclin D1/low-p27 state and had Rb
191 phosphorylated, demonstrating a critical threshold cyclin D1/p27 ratio for proliferation.
192 Strikingly, in CA-YAP cells with persistently active YAP, Rb phosphorylation remained
193 closely predicted by the relative nuclear cyclin D1 and p27 levels (Figure 2E, S2D-E), implying
194 that YAP is signaling through both cyclin D1 and p27 to control proliferation. Notably, we
195 identified some CA-YAP cells with high cyclin D1 that did not have Rb phosphorylated, but
196 these cells had increased protein levels of another CDK inhibitor, p21, which we demonstrated
197 in separate experiments (Figure 2F). Since p21 levels were only weakly regulated by serum
198 starvation or contact inhibition (Figure S2F-G), p27 is functioning as the primary proliferation
199 suppressor relevant for integrating mitogen signaling, contact inhibition, and YAP signaling[33,34].
200 The fundamental role of the cyclin D1/p27 ratio in YAP-regulated proliferation is further
201 seen in a comparison of perturbations that change the cyclin D1/p27 ratio and correspondingly
202 change Rb phosphorylation (Figure 2G). The siRNA-mediated knockdown of cyclin D1 strongly
203 reduced the proportion of cells with phosphorylated Rb by shifting most of the CA-YAP cells to a
204 high-p27 and quiescent state, but again preserved the control of Rb phosphorylation by the
205 relative cyclin D1/p27 ratio (Figure 2H, S2H). Moreover, knocking down p27 in WT cells resulted
206 in more cells ending up below the dashed line but still preserved the control of Rb
207 phosphorylation by the cyclin D1/p27 ratio (Figure 2G). Conversely, in cells where p27 levels
208 were increased by CRISPRa induction, most cells were above the relative threshold line and
209 proliferation was completely suppressed (Figure 2I). However, LATS inhibitor-mediated
210 activation of YAP in these cells lowered p27 and increased cyclin D1 to push some cells below
211 the threshold cyclin D1/p27 ratio where they could again proliferate (Figure 2I).
212 We conclude that the crucial parameter for the YAP-regulated control of cell cycle entry
213 is the nuclear cyclin D1/p27 ratio in G1 phase, with a threshold dictating whether individual cells
214 enter or exit the cell cycle (Figure 2J). Moreover, we show that there is a general convergence
215 of contact inhibition, mitogen signaling, and YAP activity, since all act through the same
216 downstream cyclin D1/p27 ratio. Notably, we were only able to identify this molecular

217 mechanism of how YAP controls the cell cycle entry and exit decision through multiplexed
218 measurements of p27, cyclin D1 and p-Rb levels within the same, G1-gated single cell.
219
220 **YAP regulation gradually changes the nuclear cyclin D1/p27 ratio**
221 We next used RNA sequencing (RNAseq) to distinguish between different potential signaling
222 pathways through which YAP activation may reversibly regulate cyclin D1 and p27 levels over
223 time. Previous studies suggested various regulatory mechanisms, such as direct induction of
224 cyclin D1[14], indirect induction of mitogen signaling[16,35], or reprogramming the cell state[15,36,37]. We
225 measured gene expression changes up to 36-hours following CA-YAP induction in low serum
226 cells (Figure 3A). Critically, we inhibited CDK4/6 activity in these cells (palbociclib) to keep cells
227 in a state with minimal E2F activation to suppress the otherwise dominating effects of the E2F
228 cell cycle transcription program that may obscure the YAP-specific transcription program.
229 We confirmed that the conserved YAP target gene signature[38] was significantly enriched
230 after 12-36 hours of induction (Figure 3B), including the canonical YAP target genes *CYR61* and
231 *ANKRD1* that were significantly induced within 6h (Figure 3C, S3B). We also confirmed
232 previously-characterized induction of G1-related target genes *CDK6*[39] and *SKP2*[40] (Figure S3B),
233 proliferation-supporting transcription factors (*MYBL1, ETS1, MYC,* Figure S3C)[15], as well as
234 TEAD and AP1 target genes[41] (*TEAD1/2*, *FOSL1/2, JUN*, Figure S3D). Compared with the fast
235 induction of the YAP target gene *CYR61*, we observed *CCND1* (cyclin D1) expression
236 increasing only after 12-36 hours and only 1.4-fold. In comparison, the previously-reported
237 suppressed gene *DDIT4*[42] rapidly dropped whereas the expression of p27 (*CDKN1B*) and p21
238 (*CDKN1A*) changed only minimally over time (Figure 3D).
239 Since there was only a small fold change in cyclin D1 and p27 expression, we next
240 tested whether cyclin D1 and p27 are more strongly regulated at the protein level[43,44] following
241 acute YAP-TEAD activation. LATS inhibitor treatment of serum-starved WT cells increased the
242 n/c YAP ratio and we confirmed the protein-level increase of select YAP targets (CDK6 and
243 SKP2, Figure S3E). LATS inhibition strongly increased cyclin D1 protein levels but also resulted
244 in a small increase in p27 and transient decrease in p21 (Figure 3E, S3F). Over 3-12 hours
245 following LATS inhibition (LATSi), the increase in the cyclin D1/p27 ratio was paralleled by
246 increasing Rb phosphorylation (Figure 3F-G), and cells progressed to S-phase within 12-24
247 hours (Figure S3G). Supporting that LATS1/2 signal through YAP-TEADs, TEAD inhibition
248 reversed the LATSi-induced changes of these protein levels and reversed the percent of
249 proliferating cells back to control levels (Figure 3F, S3G).

250 We next inhibited TEAD in proliferating cells to determine how YAP-TEAD inhibition
251 regulates cyclin D1 and p27 levels and Rb phosphorylation in G1 phase to terminate
252 proliferation. We first confirmed that TEAD inhibition of CA-YAP cells, or of LATSi pre-treated
253 WT cells, rapidly reduced the YAP ratio within 3 hours (Figure S3H). Markedly, however, TEAD
254 inhibition resulted in only a delayed reduction of the nuclear level of cyclin D1 protein in G1
255 phase (Figure 3H). Moreover, TEAD inhibition caused a strong and slow increase of the nuclear
256 protein levels of p27 and a relatively smaller increase in p21 levels across the population.
257 Concordantly, the mean cyclin D1/p27 ratio and the G1 phase Rb phosphorylation both
258 decreased but only after a delay with most cells arresting by 24-36 hours (Figure 3I, S3I).
259 Moreover, single-cell analysis confirmed that the cyclin D1/p27 ratio still predicted whether Rb
260 was phosphorylated in G1 as individual cells gradually reduced their cyclin D1 and increased
261 their p27 level (Figure 3J).
262 To more directly measure the delay between LATS and TEAD inhibition and the decision
263 in G1 whether to enter the next cell cycle after mitosis, we used live-cell analysis of
264 asynchronously dividing cells expressing a reporter of CDK2 activity[45]. CDK2 activity in cycling
265 cells bifurcates within a few hours after mitosis, distinguishing cells that enter the next cell cycle
266 from cells that stay in G1 phase[24]. We first computationally aligned cells by the time they exited
267 mitosis to compare subsequent cell cycle entry. We then measured the fraction of cells with high
268 CDK2 activity at 3 hours into G1 phase and binned them by the duration of LATS or TEAD
269 inhibition (Figure 3K).
270 To measure the effect of the inhibitor treatment as a function of time, we normalized the
271 fraction of cells with high CDK2 activity in inhibitor-treated cells to the fraction in control cells to
272 compare the relative effect of LATS or TEAD inhibition on the timing of cell cycle entry or exit.
273 This analysis showed that LATS inhibition increased the fraction of cells activating CDK2 about
274 6-fold over 24 hours, while TEAD inhibition after a short delay decreased the fraction of cells
275 about 6-fold over 24 hours (Figure 3L, S3J-K).
276 Thus, rather than inducing acute changes in cell cycle entry, YAP activation and
277 inactivation regulate the cyclin D1/p27 ratio, Rb phosphorylation, and cell cycle entry gradually
278 over a period of 24 hours. The slow kinetics of the regulation of cell cycle exit suggests that YAP
279 is regulating the cyclin D1/p27 ratio and proliferation mostly indirectly. This raises the question
280 of what mechanism mediates this slow acting component of YAP-regulated cell cycle control.
281
282 **YAP activation induces and prolongs proliferation by increasing EGFR signaling**

283 Our RNAseq time course analysis supported earlier studies that YAP activation increases
284 multiple factors related to receptor signaling[16,46–48] (Figure 4A, S4A). These factors included
285 receptors and secreted ligands known to regulate cell proliferation including *ERBB3* and *AXL*
286 receptors[3], along with ligands like *FGF1/2* and the EGFR ligand precursor *HBEGF* (paralog of
287 *AREG*)[35,49], providing a potential cell autonomous activation of EGFR and other receptors. We
288 were intrigued by this possibility since the slow kinetics of the expression changes matched the
289 delay in the changes of the cyclin D1/p27 ratio in the G1 phase after TEAD inhibition.
290 Since expression levels of *AXL* (a direct YAP target gene)[15,50,51], *EGFR,* and *HRAS* were
291 all gradually increased by YAP activation, along with the EGFR-activating ligand *HBEGF* (Figure
292 4B), we first considered whether the residual proliferation observed in serum starved cells at low
293 local density might be induced by YAP through activation of EGFR signaling. We observed that
294 the small portion of WT cells proliferating in the absence of mitogens could be inhibited by
295 titration of the EGFR inhibitor gefitinib, even in the absence of exogenous EGF (Figure 4C). This
296 EGFR inhibition mirrored the TEAD inhibition (Figure S1F), supporting that YAP-TEAD activity
297 may signal through EGFR at low stimulation conditions to promote proliferation. Nevertheless,
298 EGFR inhibition in CA-YAP cells could only partially suppress Rb phosphorylation (Figure 4E,
299 Figure S4B), suggesting that additional receptor signaling pathways are contributing to the YAP-
300 induced proliferation.
301 We next determined how rapidly TEAD inhibition changes the protein level of EGFR
302 relative to its established target AXL. Western blot analysis revealed that their total levels
303 gradually decreased after TEAD inhibition in CA-YAP cells over a similar time scale as the loss
304 of proliferation (Figure 4D). Since EGFR protein levels were YAP-dependent, we further tested
305 whether YAP activation increases EGF sensitivity. Indeed, while EGF stimulation caused only a
306 small increase in Rb phosphorylation in WT cells, Rb phosphorylation was much more strongly
307 increased in CA-YAP cells (Figure 4E). Furthermore, while both WT and CA-YAP cells had
308 similarly low basal AKT and ERK phosphorylation, the CA-YAP cells kept their phosphorylated
309 AKT and ERK levels higher for at least 10 hours after EGF stimulation compared to WT cells,
310 again consistent with sensitized EGF signaling (Figure 4F). As a control, we also confirmed that
311 TEAD inhibition of CA-YAP cells prevented this prolonged AKT and ERK signaling.
312 Finally, we tested whether there is an extended period of enhanced EGF signaling also
313 after transient LATS inactivation upstream of YAP. We used WT cells pre-treated with LATSi
314 and then either maintained (sustained) or washed out the LATSi prior to a 14-hour addition of
315 EGF (Figure 4G). While LATSi washout reduced the n/c YAP ratio and nuclear YAP levels back
316 to control conditions (Figure 4G, S4C), cells retained sensitivity to EGF for at least 14 hours, as

317 evidenced by the increased p-Rb (Figure 4H, Figure S4D), S6 phosphorylation (p-S6, a readout
318 of PI3K/mTOR activity, Figure 4I, S4E), and nuclear Fra1 levels (a YAP target but also a
319 readout of integrated MEK-ERK activity[52], Figure 4J). In support of a general prolongation of
320 proliferation signaling, we also found that transient LATSi treatment sustained the fraction of G1
321 cells with phosphorylated Rb after HGF or lysophosphatidic acid (LPA) stimulation (Figure S4F).
322 We conclude that YAP activity increases the activity of EGFR in the absence of added
323 EGF in an autocrine manner[16,49], while also increasing the sensitivity of cells to exogenous EGF
324 stimulation. This sensitization extends to other receptors since gefitinib could only suppress a
325 fraction of the YAP-induced proliferation levels and LATS-inhibited cells were more proliferative
326 following treatment with other mitogens. Notably, we showed that increased EGFR signaling
327 persisted for over 14 hours after YAP inactivation, suggesting that YAP is inducing a prolonged
328 proliferation response since its inactivation only terminates proliferation and signaling after a
329 delay.
330
331 **YAP activation signals primarily through MEK-ERK to increase the cyclin D1/p27 ratio**
332 We next examined which signaling pathways downstream of the YAP-induced receptor
333 activation control the cyclin D1/p27 ratio. We focused on PI3K-AKT-mTOR and MEK-ERK
334 signaling[46,53], since various functions of YAP activation are mediated through mTOR
335 activation,[54,55] and both mTOR and MEK-ERK can regulate cyclin D1 and p27 levels[18,33,56]
336 (Figure 5A). We measured phosphorylation of AKT and S6 protein (p-S6) to monitor PI3K
337 pathway activity and protein levels of the transcription factor Fra1 to monitor the ERK pathway.
338 Serum-starved CA-YAP cells displayed both elevated p-AKT(S473) and p-S6(240/244) as well
339 as Fra1 levels (Figure 5B-C), which similarly depended on YAP-TEAD activity, as TEAD
340 inhibition reduced their phosphorylation and protein levels in CA-YAP cells (Figure 5D).
341 To assess the functional importance of PI3K-AKT-mTOR signaling, we inhibited PI3K
342 (LY-294002) or AKT (MK2206), which had only small inhibitory effects on Rb phosphorylation in
343 CA-YAP cells (Figure 5E), despite reducing the p-AKT(S473) and p-S6(240/244 and 235/236)
344 levels (Figure S5A-B). Nevertheless, inhibiting mTORC1/2 (mTORi, Torin2) caused an
345 approximately 50% reduction in proliferation (Figure 5E). In contrast, inhibition of the obligate
346 upstream regulator of ERK, MEK (MEKi, PD0325901), completely suppressed Rb
347 phosphorylation and readouts of ERK activity (Figure 5F, S5C-D).
348 In support of YAP regulating cyclin D1 protein levels in G1 phase through mTOR and
349 MEK/ERK, rather than doing so directly, MEK inhibitor alone (Figure S5D) or the combined
350 inhibition of MEK and mTOR fully reduced the cyclin D1 level in CA-YAP cells to the level of WT

351 cells (Figure 5G, S5E). A time course analysis showed that the drop in cyclin D1 levels is rapid
352 after mTOR inhibition but slower and stronger after MEK inhibition even though both inhibitors
353 rapidly suppressed p-S6 and p-ERK, respectively (Figure 5H-I). As mTOR can rapidly control
354 translation of cyclin D1 mRNA[57], this fast regulation was anticipated. In contrast, mTOR
355 inhibition did not alter p27 levels but MEK inhibition not only reduced cyclin D1 levels but also
356 slowly and strongly increased p27 levels, explaining why MEK inhibition suppresses YAP-
357 dependent Rb phosphorylation more completely than the regulation of mTOR. Thus, transient
358 YAP-mediated proliferation responses result from an increase and delayed decrease of the
359 activity of EGFR and other receptors, which in turn transiently increases the cyclin D1/p27 ratio
360 through reversibly regulating MEK-ERK and, to a lesser degree, mTOR signaling pathways.
361

362 **Partial activation of YAP from ablating Merlin can be reversed by increased contact**
363 **inhibition**

364 Previous studies suggested that EGFR signaling and contact inhibition of proliferation are also
365 regulated independently of YAP through regulation of an upstream Hippo pathway activator,
366 Merlin/NF2[58–60]. We were particularly intrigued to study Merlin since its genetic loss increases
367 tissue size but with conflicting reports on the relevance of YAP signaling versus mitogen
368 responses. We generated clonal Merlin knockout RPE1 cells (Merlin KO) using CRISPR/Cas9
369 and confirmed that these cells had increased nuclear localization of YAP that could be
370 suppressed by TEAD inhibition (Figure S6A-B).
371 Strikingly, unlike CA-YAP, Merlin KO increased proliferation without abolishing contact
372 inhibition of proliferation. Instead, a higher cell density was required to inhibit proliferation
373 compared to WT, both at low and high serum levels (Figure 6A, S6C). Moreover, inhibiting
374 TEAD in Merlin KO cell suppressed Rb phosphorylation in both cases to levels similar as TEAD-
375 inhibited WT cells (Figure S1F), supporting a model whereby Merlin regulates proliferation
376 primarily through YAP-TEAD activity[9]. Crucially, YAP activity in Merlin KO cells could be as
377 effectively inhibited by contact inhibition as in WT cells but required a higher local cell density to
378 reach the same YAP inhibition (both at low and high serum levels, Figure 6B).
379 We next examined the role of EGFR in the Merlin KO cells, as a possible mechanism
380 mediating serum-independent proliferation downstream of the higher YAP signaling. Like CA-
381 YAP cells, Merlin KO cells displayed activated EGFR signaling in the absence of added EGF,
382 since the EGFR inhibitor gefitinib partially reduced the percentage of proliferating cells (Figure
383 6C, S6D). Like the transiently LATS-inhibited cells, the Merlin KO cells had increased sensitivity
384 to EGF while still retaining a strong local cell density dependence (Figure 6D). In addition, we

385 found that Merlin KO cells increased proliferation in response to other receptor tyrosine kinase
386 ligands (HGF and FGF, Figure S6E), again consistent with YAP inducing a broad upregulation
387 of receptor sensitivity that is not limited to EGFR.
388 Finally, we found that Merlin KO cells still suppressed cyclin D1 and increased p27
389 levels at higher local cell density (Figure 6E, S6F), demonstrating that these cells suppress
390 proliferation through the same mechanism as WT cells: inhibiting YAP activity and
391 downregulating mitogen signaling and the cyclin D1/p27 ratio. However, Merlin KO cells employ
392 alternative mechanisms from inactivating Merlin[61,62] to contact inhibit YAP.
393 We conclude that even though constitutive YAP activation abolished contact inhibition of
394 proliferation, cells can robustly contact inhibit YAP-TEAD even if Hippo signaling is reduced and
395 YAP activation increased. These studies also support that Merlin signals through YAP to control
396 EGFR and other receptor signals that together control the cyclin D1/p27 ratio. However, cells
397 that have such an induced YAP activity now require higher local cell density to suppress YAP
398 activity and proliferation.
399
400 **DISCUSSION**
401 Our study shows that contact inhibition of YAP and mitogen signaling control the cyclin D1/p27
402 ratio and cell cycle entry in G1 phase through a balance mechanism that shapes an intrinsically
403 transient YAP-induced proliferation response (Figure 6F). Our study supports a model where
404 YAP activation controls proliferation by gradually increasing the expression of HB-EGF and
405 other RTK ligands, but also various growth factor receptors and known regulators of mitogen
406 signaling[3,54,63] that mediate signal sensitivity and duration. This regulation explains how YAP
407 activation is increasing EGF and other mitogen signals in a cell autonomous manner (Figure
408 4C), while simultaneously sensitizing cells to exogenous stimulation by EGF and other mitogens
409 (Figure S4F, S6E), which is likely relevant for the role of YAP activation in the inflammatory
410 injury response[64,65]. We further show that YAP activation increases downstream signaling
411 through MEK-ERK signaling and, to an unexpectedly lesser degree, mTOR signaling, to control
412 the nuclear protein levels of cyclin D1 and p27 (Figure 5I). Most importantly, our study reveals a
413 predominant role of both cyclin D1 and p27 in YAP-induced proliferation. We showed that YAP-
414 stimulated cells decide in the G1 phase whether to enter the cell cycle by increasing the nuclear
415 cyclin D1/p27 ratio above a critical activity threshold, or to remain quiescent or exit the cell cycle
416 by staying below this threshold (Figures 2D-E, 3G,J).
417 Moreover, as the YAP-induced cell division increases the local cell density, we show that
418 the ensuing contact inhibition of YAP-TEAD causes a delayed inhibition of mitogen signaling,

419 which lowers the cyclin D1/p27 ratio to terminate the proliferation response. Thus, there are two
420 delay mechanisms ensuring that the proliferation response is prolonged: cells wait to inhibit YAP
421 until cell division has increased the local cell density, then the resulting contact inhibition of YAP
422 lowers the cyclin D1/p27 ratio and arrests proliferation after a delay (Figure 6G). YAP signals
423 often fluctuate[66–68], and the slow integration of YAP signals further ensures that the proliferation
424 response is robustly started and ended. Slow integration provides a filter mechanism which
425 prevents short-lived YAP activity changes from triggering unwanted cell cycle entry or
426 premature cell cycle exit.
427 We also evaluated the robustness of YAP inactivation by using ablation of Merlin/NF2, a
428 suppressor of Hippo signaling to YAP[69–71]. While Merlin has been shown to have additional
429 signaling functions at the plasma membrane, our study shows that the increased EGFR
430 signaling and proliferation in Merlin KO cells can be reversed by TEAD inhibition (Figure 6A),
431 suggesting that Merlin primarily signals through YAP-TEAD to control EGFR signaling, the
432 cyclin D1/p27 ratio, and proliferation. In support that the termination of YAP signaling and
433 proliferation is robust, our study shows that contact inhibition is merely shifted but not abolished
434 when YAP activity is increased by ablation of Merlin, and cells can still effectively terminate
435 proliferation but at higher local cell density. Moreover, since the loss of Merlin can boost
436 proliferation without a loss of contact inhibition, this result further suggests that Merlin has a
437 unique advantage as a drug target, since a potential Merlin inhibitor would trigger a self-limiting
438 proliferation response. This could offer a safer alternative strategy to LATS inhibition, which was
439 recently shown to cause a widespread and uncontrolled proliferation response and de-
440 differentiation in mice[6].
441 We also found that inhibiting MEK-ERK, rather than mTOR, in CA-YAP cells greatly
442 reduces the cyclin D/p27 ratio and stops proliferation. This crucial role of MEK-ERK in YAP-
443 induced proliferation was surprising, since oncogenic YAP mutants can drive resistance to
444 KRAS inhibition and KRAS primarily regulates proliferation through MEK-ERK and mTOR
445 activation[28,46,72]. The resistance to KRAS inhibitor may therefore by mediated by YAP-mediated
446 direct regulation of cell cycle entry. We confirmed that YAP activation can also directly induce
447 cyclin D1 as well as SKP2, which can degrade p27[73,74]. Indeed, we found that this upregulation
448 may be particularly important at high levels of YAP activation[75,76], since DOX induction of CA-
449 YAP in high serum conditions can still increase cyclin D1 and proliferation when MEK is
450 inhibited (Figure S6G-H).
451
452 **Concluding remarks**

453 YAP activation must be transient to drive the epithelial regenerative response without excessive
454 hyperplasia. Our study identifies a delayed, self-limiting control mechanism that allows YAP to
455 trigger such a commensurate proliferation response. We show that transient proliferation
456 responses are initiated by YAP activation increasing EGFR and mitogen signaling to increase
457 the cyclin D1/p27 ratio above a critical threshold. The delayed contact inhibition-mediated
458 inactivation of YAP then terminates proliferation by gradually lowering mitogen signaling and the
459 cyclin D1/p27 ratio below this critical threshold (Figure 6G). In contrast, we demonstrate that
460 persistent inactivation of LATS1/2 or activation of YAP activity abolishes contact inhibition and
461 promotes persistent mitogen signaling that keeps the cyclin D1/p27 ratio high, explaining how
462 oncogenic mutations that constitutively inactivate LATS1/2 or activate YAP elicit unrestricted
463 proliferation.
464

465 **Acknowledgments**
466 We thank Nathaniel Kastan and James Hudspeth for early access to a previous iteration of the
467 LATS1/2 inhibitor (TRULI); Alexander Pfannenstein, Marielle Koeberlin, and Sanjeev Sharma
468 for technical support; the Stanford Shared FACS Facility and Weill Cornell FACS Facility for cell
469 sorting; the Weill Cornell Genomics Core for library prep and RNA-sequencing; Marielle
470 Köberlin for critical reading of the manuscript; and James Ferrell, Alexander Dunn, Daniel
471 Jarosz, Ovijit Chaudhuri, Elizabeth Kiddie, members of the Meyer and Teruel laboratories for
472 technical feedback and helpful discussions. This work was funded by an NIH T32 training grant
473 (5 T32 GM 113854-3), NIH grants T.M. (R35 GM12702601) and M.N.T. (R01 DK131432);
474 K.R.F. was supported by an NSF Graduate Research Fellowship (DGE-1656518).
475

476 **Author contributions**
477 Conceptualization, K.R.F., Y.F., and T.M.; Methodology, K.R.F., N.R., Y.F., and T.M.;
478 Experiments, visualization, and analysis, K.R.F.; Manuscript preparation, K.R.F., M.N.T., and
479 T.M.; Funding acquisition, T.M., and M.N.T.
480

481 **Declaration of interests**
482 The authors declare no competing interests.
483

484 **Resource availability**
485 Immunofluorescence protocols, and cell lines are available upon request to the lead contact.
486 Plasmids generated in this study will be deposited to Addgene.

487

488 **Data and code availability**

489 MATLAB image-processing scripts and iterative imaging analysis pipeline are previously
490 published[22,77] and publicly available on Github (https://github.com/MeyerLab/image-analysis-
491 ratnayeke-2022).

492 Additional information is available upon request from the lead contact.

493

494 **Supplemental information titles and legends**

495 Figures S1-S6 and Tables S1-S2

496

497 **METHODS**

498 **Cell culture**

499 All experiments were performed with human retinal pigmented epithelial cells (RPE1-hTERT
500 immortalized, ATCC Cat# CRL-4000) unless specified otherwise. RPE1 were cultured in
501 DMEM/F12 growth media with HEPES (Thermo Scientific Cat#11039047), supplemented with
502 10% fetal bovine serum (Millipore Sigma Cat#F4135-500ML) and passaged using trypsin-EDTA
503 (0.05%, Gibco Cat# 25300054). Human mammary epithelial cells (MCF10A, ATCC Cat# CRL-
504 10317, RRID:CVCL_0598) were cultured in DMEM/F12 growth media with HEPES
505 supplemented with 5% horse serum (Gibco Cat# 16050122), 20 ng/mL EGF (PeproTech Cat#
506 C8052), 0.5 µg/mL hydrocortisone (Sigma Cat#H0888), 100 ng/mL cholera toxin (Sigma Cat#
507 C8052), and 10 µg/mL insulin (Sigma Cat#I1882). For serum starvation experiments, cells were
508 first washed with serum-free DMEM/F12 media, then maintained in serum-free (0%) or 0.1%
509 serum-containing DMEM/F12 (serum-starvation conditions). 0.1% serum-containing media had
510 similar proliferation as 0% serum-containing media, but cells were slightly more adherent to
511 glass-bottom plates for subsequent immunofluorescence protocols and therefore used for a
512 subset of experiments. For mitogen-release experiments, mitogens and growth factors (EGF,
513 HGF, and FGF at 25 ng/mL and LPA at 1 µM) were diluted in starvation media. HEK-293T cells
514 used for lentivirus production were cultured in DMEM growth media (Gibco Cat# 11995065)
515 supplemented with 10% fetal bovine serum. Cells were cultured at 37 °C and 5% CO2.

516

517 **Plasmid generation**

518 pSpCas9(BB)-2A-Puro (PX459) V2.0 was a gift from Feng Zhang (Addgene # 62988,
519 RRID:Addgene_62988). Phosphorylated and annealed sgRNA oligos against *NF2* (see Cell line
520 generation below) were cloned into restriction enzyme-digested PX459[78].

521 pQCXIH-Myc-YAP-5SA was a gift from Kun-Liang Guan (Addgene #33093, RRID:
522 Addgene_33093). Doxycycline-inducible, myc-epitope-tagged CA-YAP (YAP5SA) was
523 generated using Gibson assembly of PCR-amplified myc-YAP5SA with restriction enzyme-
524 digested plasmid backbone derived from a bicistronic vector with a TetOn promoter driving
525 target gene expression and PGK-driven rtTA expression, pCW-Cas9 (Addgene #50661, RRID:
526 Addgene_50661, a gift from Eric Lander and David Sabatini).
527
528 **Cell line generation**
529 Merlin knockout cells were generated by transient transfection of parental RPE1 cells with
530 pX459 (2 ng/uL, containing gRNA scaffolds targeting Merlin/Nf2) and Lipofectamine 2000
531 (1:500, Thermo Cat# 11668019) in Opti-MEM (Fisher Scientific Cat#31-985-070) and growth
532 media overnight, then exchanged for growth media with puromycin selection (10 µg/mL,
533 Invivogen Cat#ant-pr-1) for 72h. After a recovery period in selection-free media, cells were
534 diluted to 0.5 cells/100 µL and seeded to 96-well plates for single-cell clonal expansion. 24
535 single-cell clones were further expanded for preliminary knockout assessment by western blot
536 for loss of Merlin protein expression. 2 clones (Merlin KO-clone 1 forward:
537 CACCGCACAGTGGCCTGGCTCAAAA, reverse: AAACTTTTGAGCCAGGCCACTGTGC ;
538 Merlin KO-clone 2 forward: CACCGTGATTTGGTGTGCCGGACTC, reverse:
539 AAACGAGTCCGGCACACCAAATCAC) were selected for validation by genomic DNA
540 purification (Qiagen CAT#69504), PCR of the Merlin locus and sequencing. After initial
541 characterizations confirming Merlin KO-clone 1 and Merlin KO-clone 2 were similarly
542 proliferative (data not shown), we proceeded to use KO-clone 1 for all subsequent experiments
543 in this study.
544 Lenti-EF1a-dCas9-VPR-Puro (Addgene # 99373, RRID: Addgene_99373) was a gift
545 from Kristen Brennard and stably expressed in RPE1 cells using puromycin selection (10
546 ug/mL, Invivogen Cat#ant-pr-1). CA-YAP and dCas9-expressing cells were generated using
547 third-generation lentiviral transduction. Lentivirus was generated in HEK-293T cells by
548 transfection with packaging and envelope plasmids pMDLg/pRRE (Addgene # 12251, RRID:
549 Addgene_12251), pRSV-rev (Addgene #1225, RRID: Addgene_1225), and pCMV-VSV-G
550 (Addgene #8454, RRID: Addgene_8454) in Lipofectamine 2000 and Opti-MEM. After 72h
551 transfection, supernatant was passed through a 0.22 uM filter (Millipore Cat# SCGP00525) and
552 concentrated using 100 kDa centrifugal filters (Millipore Cat# UFC910024). Lentivirus was then
553 frozen or directly transduced into cells. 72h after lentiviral transduction, cells were split into
554 antibiotic-selection media or, if expressing a fluorescent construct, expanded prior to sorting by

555 a BD Influx cell sorter (Stanford Shared FACS Facility, Weill Cornell FACS Facility). RPE1
556 reporter cell lines were generated by transduction with pLV-H2B-miRFP670 (nuclear marker),
557 CSII-pEF1a-hDHB(994-1087)-mTurquoise (cyclin E/A-CDK reporter), and the FUCCI cell-cycle
558 reporters CSII-pEF1a-mVenus-hGeminin(1-110) (APC/C^{Cdh1} reporter) and pLV-mCherry-
559 hCDT1(1-100)ΔCy (S-phase start[79]), as described previously[77].
560
561 **siRNA, sgRNA, and plasmid transfection**
562 All oligo sequences are listed in Table S1. Pooled siRNA (ON-TARGETplus, Horizon Discovery
563 Biosci.) were used for siCtrl (Non-targeting Control, Horizon Cat#D-001810-10-05), siCycD1
564 (siCCND1, Horizon Cat# L-003210-00-0005), and sip27 (siCDKN1B, Horizon Cat# L-040178-
565 00-0005). For CRISPRa-mediated overexpression of genes through targeting of endogenous
566 promoters, pooled sgRNA (Horizon) were used for sgCtrl (non-targeting control, Horizon Cat#
567 U-009500-10-05), sgCycD1 (sgCCND1, Horizon Cat# P-003210-01-0005), and sgp27
568 (sgCDKN1B, Horizon Cat# P-003472-01-0005) with tracRNA (Edit-R tracrRNA, Cat# U-002005-
569 05). RPE1 cells were transfected with siRNA and sgRNA using DharmaFECT 1 (1:500 in Opti-
570 MEM, Dharmacon Cat# T-2001-03) according to manufacturer protocol using 20 nM siRNA, or
571 sgRNA and tracrRNA (in 1:1 ratio, according to manufacturer protocol). Cells were incubated in
572 transfection mixture for 6-12h in growth media, then replaced with media appropriate for the
573 experiment conditions and assessed 24-48h after transfection.
574
575 **Drugs and mitogens**
576 Human growth factors and mitogens were dissolved in sterile, ultrapure water (Fisher Scientific
577 Cat#10977023) and used at the following concentrations unless otherwise stated: 25 ng/mL
578 recombinant EGF (PeproTech cat#AF-100-15), 25 ng/mL recombinant HGF (Life Technologies
579 Cat#PHG0254), 25 ng/mL recombinant FGF basic (R&D Systems Cat#233-FB-025), 1 uM LPA
580 (oleoyl-L-alpha-lysophosphatidic acid, Sigma-Aldrich Cat#L7260-1MG).
581 Drugs were dissolved in DMSO (Sigma-Aldrich Cat# D2650) and used at the following
582 concentrations unless otherwise stated: 0.5 μM TDI-011536 (Selleck Chemicals Cat#E1314,
583 CAS#2687970-96-1, LATSi), 5 μM TRULI (a gift from James Hudspeth, CAS#1424635-83-5), 1
584 μM GNE-7887 (ChemieTek Cat#CT-GNE7883, CAS# 2648450-42-2,TEADi), 10 μM gefitinib
585 (Selleck Chemicals Cat#S1025, CAS#184475-35-2, EGFRi), 10 μM LY294002 (Cayman
586 Chemical Cat#70920, CAS#154447-36-6 , PI3Ki), 200 nM MK2206 (Cayman Chemical
587 Cat#11593, CAS#1032350-13-2, AKTi), 100 nM Torin2 (Cayman Chemical Cat#14185,
588 CAS#1223001-51-1, mTORi), 100 nM PD0325901 (Selleck Chemicals Cat#S1036,

589 CAS#391210-10-9, MEKi), 1 μM palbociclib (PD-0332991, Selleck Chemicals cat#S1116,
590 CAS#827022-32-2, CDK4/6i), 0.5 ug/mL doxycycline hyclate (Sigma-Aldrich cat#D9891,
591 CAS#24390-14-5, DOX), 10 μM 5-ethynyl-2'-deoxyuridine (EdU, Cayman Chemical Cat#20518,
592 CAS# 61135-33-9). For drug treatments and time courses, control conditions were treated with
593 DMSO, except mitogen release controls (mock), which were dissolved in water. For all EdU-
594 incorporation, cells received an EdU spike-in (10 μM, in serum-free media) for 12-15 min prior to
595 fixation.
596
597 **Western blotting**
598 Cells grown in 6-well plates were washed once in cold, sterile PBS and lysed in chilled, 1x RIPA
599 buffer (Boston BioProducts Cat#BP-115-5X) or non-denaturing lysis buffer (20 mM HEPES, 150
600 mM NaCl, 2 mM EDTA, 0.1% IGEPAL-CA630) containing HALT protease and phosphatase
601 inhibitor cocktail (1:100, Thermo Fisher Cat#78439). Lysates were harvested on ice using cell
602 scrapers, sheared by syringe (25G) and centrifuged at 15,000 RCF for 15 min at 4C.
603 Supernatant was stored at -20C. Protein concentration was calculated by Pierce BCA Protein
604 Assay (Thermo Fisher Cat#23225) according to manufacturer protocol and a BSA standard
605 curve.
606 10-30 ug protein was loaded onto 7.5%, 12%, or 4-20% Mini-PROTEAN TGX gels for
607 resolution by SDS-PAGE in 1x Laemmli sample buffer (Fisher Scientific, Cat#AAJ60660AC, or
608 Bio-Rad Cat#1610737) alongside Page RulerPlus (Thermo Scientific Cat#26620) molecular
609 ladders in Tris/Glycine/SDS running buffer (Bio-Rad Cat#161-0772). Gels were run at 150V for
610 1h then transferred to 0.2 um PVDF membranes by semi-dry transfer (Bio-Rad Trans-Blot SD,
611 Cat# 1703940) in Tris/Glycine buffer (Bio-Rad Cat# 1610734) with 10% methanol, or semi-dry
612 transfer (Bio-Rad Trans-Blot Turbo Cat# 1704150) with Trans-Blot Turbo Transfer Packs (Bio-
613 Rad Cat# 1704156). Membranes were washed in TBST (20 mM Tris, pH 7.5, 150 mM NaCl,
614 0.1% Tween-20), blocked for 30 min in 5% milk/TBST (VWR Cat#10128-602), and incubated at
615 RT for 3h or overnight at 4C in primary antibody dilutions in 5% BSA/TBST + 0.01% NaN3.
616 Primary antibodies used were rabbit anti-AXL (1:1000, Cell Signaling Technology Cat# 8661,
617 RRID:AB_11217435), rabbit anti-EGFR (1:1000, Cell Signaling Technology Cat# 4267,
618 RRID:AB_2246311), rabbit anti-GAPDH (1:1000, Cell Signaling Technology Cat# 5174,
619 RRID:AB_10622025), mouse anti-Vinculin (1:1000, Thermo Fisher Scientific Cat# 14-9777-80,
620 RRID:AB_2573027), rabbit anti-Merlin (1:1000, Cell Signaling Technology Cat# 12888,
621 RRID:AB_2650551) (see also Table S2).

622 After 2x washes in TBST, membranes were incubated with anti-rabbit or anti-mouse
623 HRP-conjugated secondary antibodies (1:5000, CST#7074, RRID: AB_2099233 or CST#7076,
624 RRID: AB_330924) or fluorophore-conjugated secondary antibodies (1:10,000, LI-COR
625 Biosciences, IRDye 680 LT CAT#925-68020, or IRDye 800CW, CAT#925-32210) in 5%
626 BSA/TBST for 1h at RT. Membranes treated with enhanced chemiluminescence substrate
627 (Thermo Fisher Cat#PI34080) were detected by film (Thomas Sci. Cat#EK-5130) or Licor
628 Odyssey Fc. Membranes treated with fluorophore-conjugated secondary antibodies were
629 imaged on a Licor Odyssey Fc. Normalized protein level changes were calculated using FIJI [80]
630 by measuring the integrated intensity of a set box size encompassing the protein band. The
631 background signal was measured by applying the same box to an adjacent region of the blot
632 and subtracted from the median protein intensity. An equivalent box size was used for
633 reference/loading control protein bands as the protein of interest.
634
635 **Immunofluorescence**
636 Cells were plated on bovine fibronectin-coated (1:75 in PBS, Sigma-Aldrich F1141,
637 CAT#F1141) or collagen-coated (1:100 in PBS, Advanced Biomatrix Cat#5005-B), 96-well,
638 glass-bottom plates (Cellvis CAT# P96-1.5h-N). Cells were fixed in 4% PFA (in PBS, Fisher
639 Scientific Cat#AA433689) for 15 min at room temperature (RT), washed 3x with PBS,
640 permeabilized in 0.2% Triton X-100 for 15 min, and blocked in blocking solution (10% FBS, 5%
641 BSA, 0.1% Triton X-100, 0.01% NaN3 in PBS) for 1h at RT. For conditions with EdU
642 incorporation (10 μM in basal medium, 12-15 min at 37C, Cayman Chemical Cat#20518) prior
643 to fixation, cells were washed 1x with PBS after the blocking step and treated with a click
644 chemistry solution (2 mM CuSO4, 20 mg/mL sodium ascorbate, 3 μM AFDye picolyl azide (488,
645 568, or 647, Click Chemistry Tools Cat# 1276, 1292, or 1300 respectively) in TBS (50 mM Tris,
646 150 mM NaCl, pH 8.3) for 25 min. Following a 1x PBS wash, cells were incubated with primary
647 antibody for 3h at room temperature or overnight at 4C (see also Table S2) in blocking solution,
648 then washed 3x in PBS. Fluorophore-conjugated secondary antibodies (Thermo Fisher
649 Scientific, goat anti-mouse, goat anti-rabbit, 1:1000 in blocking solution) and Hoechst 333342
650 (Thermo Fisher Scientific Cat#H3570, 1:10,000) were incubated on cells for 1h at RT, then
651 washed 3x in PBS. Wells were imaged in 1x PBS or 1x N-acetylcysteine (NAC, 700 mM in
652 ddH2O, pH 7.4, Sigma-Aldrich A7250) imaging buffer for iterative immunofluorescence
653 protocol[32] (4i).
654 For the 4i protocol, wells were then washed 1x in dH2O, treated with elution buffer (0.5M
655 L-glycine (Sigma-Aldrich Cat#G2879), 3M urea (Sigma-Aldrich Cat#U5378), 3M guanidine

656 hydrochloride (Sigma-Aldrich Cat# G3272), 70 mM TCEP-HCl (Goldbio Cat# TCEP50) in
657 ddH2O, pH 2.5) for 20 min on an orbital shaker. After 1x PBS wash, elution was confirmed by
658 fluorescence microscopy. Cells were then blocked with 4i blocking solution (1% BSA + 150 mM
659 maleimide (Sigma-Aldrich Cat# 129585) in PBS) for 30 min, then incubated with the second
660 round of primaries (in blocking solution) for at least 3h RT or overnight at 4C. Secondary
661 staining, imaging in NAC, and subsequent elution and 4i blocking steps were repeated up to 5
662 times. Control wells with secondary antibody treatment alone were used to confirm proper
663 elution of previous antibody rounds. Antibody list and dilutions used for immunofluorescence are
664 listed below and in Table S2:
665
666 **Immunofluorescence Antibodies**
667 The following primary antibodies were used exclusively for round 1 of immunofluorescence
668 staining: rabbit anti-CDK6 (1:1000, Abcam Cat#ab124821, RRID: AB_10999714), rabbit anti-
669 YAP (1:400, Cell Signaling Technology Cat# 14074, RRID:AB_2650491), mouse anti-p27
670 (1:1000, Cell Signaling Technology Cat#3698, RRID:AB_2077832), mouse anti-p21 (1:500, BD
671 Bioscience Cat#556430, RRID:AB_396414), rabbit phospho-AKT(S473)(1:400, Cell Signaling
672 Technology Cat#4060, RRID:AB_2315049), rabbit phospho-MAPK1/2(Thr202/Tyr204)(1:400,
673 Cell Signaling Technology Cat#4370, RRID:AB_2315112), mouse phospho-S6(235/236)(1:800,
674 Cell Signaling Technology Cat#62016, RRID:AB_2799618).
675 The following primary antibodies were used for any round of immunofluorescence:
676 mouse anti-cyclin D1 (1:200, Santa Cruz Biotech Cat#sc-8396, RRID:AB_627344), mouse anti-
677 FRA1 (1:200, Santa Cruz Biotech Cat#sc-28310, RRID: AB_ AB_627632), rabbit anti-Myc
678 (1:800, Cell Signaling Technology Cat#5605, RRID:AB_1903938), mouse anti-Myc tag (1:8,000,
679 Cell Signaling Technology Cat#2276, RRID:AB_331783), mouse anti-N-cadherin (1:200, Santa
680 Cruz Biotech Cat#sc-393933, RRID: AB_2832921), rabbit anti-p27 (1:1600, Cell Signaling
681 Technology Cat#3686, RRID:AB_2077850), rabbit anti-p21 (1:2500, Cell Signaling Technology
682 Cat#2947, RRID:AB_823586), rabbit anti-phospho-Rb(Ser807/811)(1:2500, Cell Signaling
683 Technology Cat#8516, RRID:AB_1117658), rabbit anti-phospho-S6(240/244)(1:2500, Cell
684 Signaling Technology Cat#5364, RRID:AB_10694233), rabbit anti-Skp2 (1:800, Cell Signaling
685 Technology Cat#2652, RRID:AB_11178941), mouse anti-YAP (1:200, Santa Cruz Biotech.
686 Cat#sc-101199,RRID: AB_1131430). Antibodies were previously validated in RPE1[22] and for
687 4i[81], and in this study by drug treatment (including AKT, mTORC1/2, MEK, and LATS1/2
688 inhibitors).

689 The following secondaries were used in variable combination (488, 514 or 568, and
690 647), at 1:1000: goat anti-mouse IgG Alexa Fluor 488 (Thermo Fisher Scientific Cat#A11029,
691 RRID:AB_2534088), goat anti-mouse IgG Alexa Fluor 514 (Thermo Fisher Scientific
692 Cat#A31558, RRID:AB_1037789), goat anti-mouse IgG Alexa Fluor 568 (Thermo Fisher
693 Scientific Cat#A-11031 RRID:AB_144696), goat anti-rabbit IgG Alexa Fluor 568 (Thermo Fisher
694 Scientific Cat#A11036, RRID:AB_1056366), goat anti-rabbit IgG Alexa Fluor 647 (Thermo
695 Fisher Scientific Cat#A21245, RRID:AB_23813).
696
697 **Microscopy**
698 For automated epifluorescence microscopy, cells were imaged on a Ti2-E inverted microscope
699 (Nikon) using penta-band (DAPI/CFP/YFP/TRITC/Cy5, Chroma: 89405) Sedat filter sets with an
700 LED light source (Lumencor Spectra X or Spectra III), Hamamatsu ORCA-fusionBT or ORCA-
701 Flash4.0 V3 sCMOS camera, and 20x objective (Nikon CFI Plan Apo Lambda, 0.75 NA) in a
702 humidified chamber at 37 ºC and 5% CO2. 25-30 tiled images were acquired per well in 16-bit
703 mode with 2x2 binning. Fixed cells were imaged in 1x N-acetylcysteine imaging buffer.
704 Fluorophores for secondary antibodies were previously optimized to minimize bleed-through[77].
705 For live-cell imaging, 9 sites were imaged per well and stitched into a single image to maximize
706 the number of cells that could be tracked over time (with at least 3 well-replicates per
707 experiment). Images were acquired at 12 min intervals of with the minimum laser intensity and
708 light exposure to limit phototoxic effects and automated shading correction for each channel
709 based on the autofluorescence of media containing 10% serum. For LATS1/2 and TEAD
710 inhibitor experiments, asynchronously cycling cells were imaged in DMSO for 12h, then acutely
711 treated with inhibitor and imaged for 24h to assess cell cycle entry and exit.
712
713 **RNA sequencing experimental conditions**
714 WT and doxycycline-inducible YAP5SA cells were seeded at 38,000 cells per well of 96-well,
715 optical-grade plates (Sigma-Aldrich Cat#CLS3904) in 1.0% FBS. After ~2h to allow time for
716 adherence to the tissue culture surface, cells were washed with 0.1% FBS then pre-arrested
717 with CDK4/6 inhibitor (palbociclib, 1 uM, SelleckChem CAT#S1116) in either 1.0% FBS or 0.1%
718 FBS for 28-36h prior to doxycycline (500 ng/mL, Sigma-Aldrich CAT#D9891) induction or
719 DMSO control treatment for 6, 12, 24, or 36h in the presence of CDK4/6 inhibitor to maintain
720 cells in G0 and prevent additional transcriptional variation due to cell cycle progression. Each
721 experiment (repeated on three separate occasions) was performed in technical duplicate (with 6
722 replicate wells per technical duplicate), reserving one replicate for immunofluorescence staining

723 to confirm quality of cell cycle arrest (by DNA content and EdU incorporation) and the other for
724 harvesting RNA.
725
726 **RNA-seq and analysis**
727 Prior to harvesting, 96-well plates were washed with PBS, aspirated fully and transferred
728 immediately to -80C. RNA was later harvested from the plates by briefly thawing prior to using
729 extraction by RNeasy Mini kit (Qiagen Cat# 74106) and QIAshredder (Qiagen Cat#79654), with
730 pooling of 6 technical replicate wells/condition directly following the lysis step prior to following
731 the manufacturer protocol, including the optional DNase treatment (Qiagen Cat# 79254).
732 Samples were eluted in ultraPure ddH2O and assessed for quality using an Agilent Bioanalyzer
733 TapeStation. Illumina Stranded mRNA library preparation with polyA capture and sequencing
734 was performed on a NovaSeq6000 system (paired-end, 2 x 50) at the Weill Cornell Genome
735 Resources Core Facility over two rounds to get sufficient read depth.
736 Raw reads were checked for quality using FASTQC then aligned to the human genome
737 assembly (GRCh38) with HISAT2[82] and assigned to genomic features with featureCounts[83].
738 Differential expression analysis was conducted with DESeq2[84].
739
740 **Image quantifications and analysis**
741 Tracking of cells for time-lapse experiments, illumination bias correction, nuclear segmentation,
742 image cropping and alignment across iterative rounds of immunofluorescence, and analysis
743 were performed with a custom MATLAB pipeline (previously published[77] and deposited on
744 Github: https://github.com/MeyerLab/image-analysis-ratnayeke-2021) incorporating local density
745 measurements[22]. For illumination bias correction, images of background autofluorescence from
746 immunofluorescence blocking solution in cell-free wells were taken for each experiment and
747 used to flatten raw images. Cell nuclei were automatically segmented using expression of a
748 fluorescently-tagged nuclear marker (H2B-miRFP670) or Hoechst staining, a Gaussian filter,
749 and a curvature-based object splitting algorithm. A segmentation mask from the first round of
750 imaging was used to align subsequent imaging rounds and crop the images for the overlapping
751 regions. Image jitter between 4i rounds was typically less than 500 nm.
752 For nuclear-localized protein stains (EdU, cyclin D1, p27, phospho-Rb, c-Myc, Fra1,
753 SKP2, CDK6, p21), global background subtraction was performed automatically by expanding a
754 7.8 μm ring from the nuclear mask and subtracting the 25th percentile of pixel signal as
755 estimated background. For protein stains with cytoplasmic and nuclear localization (YAP,
756 phospho-S6, phospho-AKT, phospho-ERK, N-cadherin), median background signal was

757 estimated during analysis by manual averaging of background pixels of representative cell-free
758 regions and subtracting as a flat threshold. For quantification of immunofluorescence signals,
759 DNA content was calculated as the total nuclear Hoechst intensity (median intensity x nuclear
760 area); nuclear fluorescence signals were calculated as the median nuclear intensity;
761 cytoplasmic fluorescence signals were calculated as the median cytoplasmic intensity
762 (expanding the nuclear mask with a ring of inner radius 0.65 um and outer radius 3.23 um to
763 minimize the chance of sampling cytoplasm of neighboring cells). To compare experimental
764 replicates, fold-change in immunofluorescence staining was used to account for the variation in
765 staining and real fluorescence unit values.
766 Cell gating for G1-phase cells was performed by distinguishing G0/G1 and G2 cell
767 populations by 2N or 4N DNA context, then selecting cells below the EdU-incorporation
768 threshold (see sample EdU histograms, Figure S1A) with 2N DNA. Otherwise, for calculating
769 percent EdU-positive or percent Rb phosphorylated (all-cell gating), cells across cell cycle
770 phases were analyzed together. Rb phosphorylation was defined by histogram analysis of the
771 bifurcated phospho-Rb stain and calculating the fraction of cells above the threshold cutoff (see
772 sample p-Rb histograms, Figure S1A).
773 For analysis of CDK2 activity at 3h following mitosis in cells with variable time spent in
774 LATS1/2 or TEAD inhibitor (Figure 3K-L cell traces were first gated based on cells that were
775 tracked for at least 20% of the total imaging time (36h) and tracked from the time of birth or
776 mitosis (denoted as a daughter cell). CDK2 activity of the kinase translocation reporter was
777 measured as a ratio of the median intensity of a cytoplasmic ring (0.65 – 3.25 μm expansion
778 from the nuclear mask) over the median intensity of the nuclear signal. For calculating the
779 fraction of cells with high CDK2 activity, asynchronously cycling cells were first binned into 3h
780 windows by time of mitosis (to ensure enough cells analyzed per time window of mitosis) and
781 then gated by time spent in the inhibitors by selecting cells that were born at variable times
782 following the switch from DMSO to the LATS or TEAD inhibitor. The fraction of cells with CDK2
783 activity above a standardized threshold (0.8) was calculated 3h after mitosis as an early
784 indicator of cells bifurcating into low or high activity[45], but similar results were also seen if
785 assessing CDK activity at 6h after mitosis (data not shown).
786
787 **Local cell density analysis**
788 Local cell density analysis was adapted from Fan et al., 2021. Briefly, local density was
789 measured by dividing imaging sites (25-30 tiled images/well) into a 3D histogram based on the
790 centroid coordinates of segmented nuclei (10 x 10 grid, MATLAB hist3). The xy location

791 coordinates of each cell centroid were rounded and the number of cells per block was
792 automatically counted, then scaled back to match the original image size (giving numerical
793 output rather than integer values)[22]. The local cell density value assigned for each cell was
794 based on the scaled number of cells in its assigned local density block.
795
796 **Quantification corrections**
797 While cells were counted prior to seeding, final cell plating density varied across experiments,
798 and absolute proliferation levels varied per independent experiment. We therefore assessed
799 both absolute (% EdU, % p-Rb) and fold-change proliferation metrics for assessing drug and
800 condition effect sizes.
801 During the iterative steps of multiplexed immunofluorescence, some cells washed off
802 during later rounds of imaging. As a proxy for null cells, cells that were segmented from the first
803 round of imaging were gated out of the final analysis if their Hoechst value was less than 100
804 RFU for a subsequent imaging round.
805 For live-cell imaging experiments, some cells lost expression of the reporters of cell
806 cycle activity and were therefore removed from analysis.
807
808 **Statistical Analysis**
809 Statistical analyses were performed using Student's one-sample or paired (MATLAB ttest) and
810 two-sample (MATLAB ttest2) t tests. Linear regressions for data binned by local cell density
811 were performed using fitlm (MATLAB). 95% confidence intervals and SEM are plotted as
812 indicated for representative experiments and summary data.
813
814 **REFERENCES**
815

816 1. Moya, I.M., and Halder, G. (2019). Hippo-YAP/TAZ signalling in organ regeneration
817 and regenerative medicine. Nat. Rev. Mol. Cell Biol. *20*, 211–226. 10.1038/s41580-018-
818 0086-y.

819 2. Driskill, J.H., and Pan, D. (2023). Control of stem cell renewal and fate by YAP and
820 TAZ. Nat. Rev. Mol. Cell Biol. *24*, 895–911. 10.1038/s41580-023-00644-5.

821 3. Totaro, A., Panciera, T., and Piccolo, S. (2018). YAP/TAZ upstream signals and
822 downstream responses. Nat. Cell Biol. *20*, 888–899. 10.1038/s41556-018-0142-z.

823 4. Fan, F., He, Z., Kong, L.-L., Chen, Q., Yuan, Q., Zhang, S., Ye, J., Liu, H., Sun, X.,
824 Geng, J., et al. (2016). Pharmacological targeting of kinases MST1 and MST2 augments
825 tissue repair and regeneration. Sci. Transl. Med. *8*, 352ra108.
826 10.1126/scitranslmed.aaf2304.

827 5. Kastan, N., Gnedeva, K., Alisch, T., Petelski, A.A., Huggins, D.J., Chiaravalli, J.,
828 Aharanov, A., Shakked, A., Tzahor, E., Nagiel, A., et al. (2021). Small-molecule
829 inhibition of Lats kinases may promote Yap-dependent proliferation in postmitotic
830 mammalian tissues. Nat. Commun. *12*, 3100. 10.1038/s41467-021-23395-3.

831 6. Namoto, K., Baader, C., Orsini, V., Landshammer, A., Breuer, E., Dinh, K.T., Ungricht,
832 R., Pikiolek, M., Laurent, S., Lu, B., et al. (2024). NIBR-LTSi is a selective LATS kinase
833 inhibitor activating YAP signaling and expanding tissue stem cells in vitro and in vivo.
834 Cell Stem Cell *31*, 554-569.e17. 10.1016/j.stem.2024.03.003.

835 7. Meng, Z., Moroishi, T., and Guan, K.-L. (2016). Mechanisms of Hippo pathway
836 regulation. Genes Dev. *30*, 1–17. 10.1101/gad.274027.115.

837 8. Gumbiner, B.M., and Kim, N.-G. (2014). The Hippo-YAP signaling pathway and contact
838 inhibition of growth. J. Cell Sci. *127*, 709–717. 10.1242/jcs.140103.

839 9. Zhang, N., Bai, H., David, K.K., Dong, J., Zheng, Y., Cai, J., Giovannini, M., Liu, P.,
840 Anders, R.A., and Pan, D. (2010). The Merlin/NF2 tumor suppressor functions through
841 the YAP oncoprotein to regulate tissue homeostasis in mammals. Dev. Cell *19*, 27–38.
842 10.1016/j.devcel.2010.06.015.

843 10. Huang, J., Wu, S., Barrera, J., Matthews, K., and Pan, D. (2005). The Hippo signaling
844 pathway coordinately regulates cell proliferation and apoptosis by inactivating Yorkie,
845 the Drosophila Homolog of YAP. Cell *122*, 421–434. 10.1016/j.cell.2005.06.007.

846 11. Benhamouche, S., Curto, M., Saotome, I., Gladden, A.B., Liu, C.-H., Giovannini, M., and
847 McClatchey, A.I. (2010). Nf2/Merlin controls progenitor homeostasis and tumorigenesis
848 in the liver. Genes Dev. *24*, 1718–1730. 10.1101/gad.1938710.

849 12. Yu, F.-X., Zhao, B., and Guan, K.-L. (2015). Hippo pathway in organ size control, tissue
850 homeostasis, and cancer. Cell *163*, 811–828. 10.1016/j.cell.2015.10.044.

851 13. Zhao, B., Ye, X., Yu, J., Li, L., Li, W., Li, S., Yu, J., Lin, J.D., Wang, C.-Y., Chinnaiyan,
852 A.M., et al. (2008). TEAD mediates YAP-dependent gene induction and growth control.
853 Genes Dev. *22*, 1962–1971. 10.1101/gad.1664408.

854 14. Mizuno, T., Murakami, H., Fujii, M., Ishiguro, F., Tanaka, I., Kondo, Y., Akatsuka, S.,
855 Toyokuni, S., Yokoi, K., Osada, H., et al. (2012). YAP induces malignant mesothelioma
856 cell proliferation by upregulating transcription of cell cycle-promoting genes. Oncogene
857 *31*, 5117–5122. 10.1038/onc.2012.5.

858 15. Zanconato, F., Forcato, M., Battilana, G., Azzolin, L., Quaranta, E., Bodega, B., Rosato,
859 A., Bicciato, S., Cordenonsi, M., and Piccolo, S. (2015). Genome-wide association
860 between YAP/TAZ/TEAD and AP-1 at enhancers drives oncogenic growth. Nat. Cell
861 Biol. *17*, 1218–1227. 10.1038/ncb3216.

862 16. Zhang, J., Ji, J.-Y., Yu, M., Overholtzer, M., Smolen, G.A., Wang, R., Brugge, J.S.,
863 Dyson, N.J., and Haber, D.A. (2009). YAP-dependent induction of amphiregulin
864 identifies a non-cell-autonomous component of the Hippo pathway. Nat. Cell Biol. *11*,
865 1444–1450. 10.1038/ncb1993.

866 17. Zhang, H., Pasolli, H.A., and Fuchs, E. (2011). Yes-associated protein (YAP)
867 transcriptional coactivator functions in balancing growth and differentiation in skin. Proc
868 Natl Acad Sci USA *108*, 2270–2275. 10.1073/pnas.1019603108.

869 18. Lavoie, H., Gagnon, J., and Therrien, M. (2020). ERK signalling: a master regulator of
870 cell behaviour, life and fate. Nat. Rev. Mol. Cell Biol. *21*, 607–632. 10.1038/s41580-020-
871 0255-7.

872 19. Chiasson-MacKenzie, C., and McClatchey, A.I. (2018). Cell-Cell Contact and Receptor
873 Tyrosine Kinase Signaling. Cold Spring Harb. Perspect. Biol. *10*.
874 10.1101/cshperspect.a029215.

875 20. Rubin, S.M., Sage, J., and Skotheim, J.M. (2020). Integrating old and new paradigms of
876 G1/S control. Mol. Cell *80*, 183–192. 10.1016/j.molcel.2020.08.020.

877 21. Zhao, B., Wei, X., Li, W., Udan, R.S., Yang, Q., Kim, J., Xie, J., Ikenoue, T., Yu, J., Li,
878 L., et al. (2007). Inactivation of YAP oncoprotein by the Hippo pathway is involved in
879 cell contact inhibition and tissue growth control. Genes Dev. *21*, 2747–2761.
880 10.1101/gad.1602907.

881 22. Fan, Y., and Meyer, T. (2021). Molecular control of cell density-mediated exit to
882 quiescence. Cell Rep. *36*, 109436. 10.1016/j.celrep.2021.109436.

883 23. Overholtzer, M., Zhang, J., Smolen, G.A., Muir, B., Li, W., Sgroi, D.C., Deng, C.-X.,
884 Brugge, J.S., and Haber, D.A. (2006). Transforming properties of YAP, a candidate
885 oncogene on the chromosome 11q22 amplicon. Proc Natl Acad Sci USA *103*, 12405–
886 12410. 10.1073/pnas.0605579103.

887 24. Yang, H.W., Chung, M., Kudo, T., and Meyer, T. (2017). Competing memories of
888 mitogen and p53 signalling control cell-cycle entry. Nature *549*, 404–408.
889 10.1038/nature23880.

890 25. Aoki, K., Kumagai, Y., Sakurai, A., Komatsu, N., Fujita, Y., Shionyu, C., and Matsuda,
891 M. (2013). Stochastic ERK activation induced by noise and cell-to-cell propagation
892 regulates cell density-dependent proliferation. Mol. Cell *52*, 529–540.
893 10.1016/j.molcel.2013.09.015.

894 26. Cai, J., Zhang, N., Zheng, Y., de Wilde, R.F., Maitra, A., and Pan, D. (2010). The Hippo
895 signaling pathway restricts the oncogenic potential of an intestinal regeneration program.
896 Genes Dev. *24*, 2383–2388. 10.1101/gad.1978810.

897 27. Lee, M.-J., Byun, M.R., Furutani-Seiki, M., Hong, J.-H., and Jung, H.-S. (2014). YAP
898 and TAZ regulate skin wound healing. J. Invest. Dermatol. *134*, 518–525.
899 10.1038/jid.2013.339.

900 28. Hagenbeek, T.J., Zbieg, J.R., Hafner, M., Mroue, R., Lacap, J.A., Sodir, N.M., Noland,
901 C.L., Afghani, S., Kishore, A., Bhat, K.P., et al. (2023). An allosteric pan-TEAD inhibitor
902 blocks oncogenic YAP/TAZ signaling and overcomes KRAS G12C inhibitor resistance.
903 Nat. Cancer *4*, 812–828. 10.1038/s43018-023-00577-0.

904 29. Kastan, N.R., Oak, S., Liang, R., Baxt, L., Myers, R.W., Ginn, J., Liverton, N., Huggins,
905 D.J., Pichardo, J., Paul, M., et al. (2022). Development of an improved inhibitor of Lats
906 kinases to promote regeneration of mammalian organs. Proc Natl Acad Sci USA *119*,
907 e2206113119. 10.1073/pnas.2206113119.

908 30. Bienvenu, F., Jirawatnotai, S., Elias, J.E., Meyer, C.A., Mizeracka, K., Marson, A.,
909 Frampton, G.M., Cole, M.F., Odom, D.T., Odajima, J., et al. (2010). Transcriptional role
910 of cyclin D1 in development revealed by a genetic-proteomic screen. Nature *463*, 374–
911 378. 10.1038/nature08684.

912 31. Koff, A. (2006). How to decrease p27Kip1 levels during tumor development. Cancer Cell
913 *9*, 75–76. 10.1016/j.ccr.2006.01.020.

914 32. Gut, G., Herrmann, M.D., and Pelkmans, L. (2018). Multiplexed protein maps link
915 subcellular organization to cellular states. Science *361*. 10.1126/science.aar7042.

916 33. Cheng, M., Sexl, V., Sherr, C.J., and Roussel, M.F. (1998). Assembly of cyclin D-
917 dependent kinase and titration of p27Kip1 regulated by mitogen-activated protein kinase
918 kinase (MEK1). Proc Natl Acad Sci USA *95*, 1091–1096. 10.1073/pnas.95.3.1091.

919 34. Polyak, K., Lee, M.H., Erdjument-Bromage, H., Koff, A., Roberts, J.M., Tempst, P., and
920 Massagué, J. (1994). Cloning of p27Kip1, a cyclin-dependent kinase inhibitor and a
921 potential mediator of extracellular antimitogenic signals. Cell *78*, 59–66. 10.1016/0092-
922 8674(94)90572-x.

923 35. Gregorieff, A., Liu, Y., Inanlou, M.R., Khomchuk, Y., and Wrana, J.L. (2015). Yap-
924 dependent reprogramming of Lgr5(+) stem cells drives intestinal regeneration and cancer.
925 Nature *526*, 715–718. 10.1038/nature15382.

926 36. Croci, O., De Fazio, S., Biagioni, F., Donato, E., Caganova, M., Curti, L., Doni, M.,
927 Sberna, S., Aldeghi, D., Biancotto, C., et al. (2017). Transcriptional integration of
928 mitogenic and mechanical signals by Myc and YAP. Genes Dev. *31*, 2017–2022.
929 10.1101/gad.301184.117.

930 37. Monroe, T.O., Hill, M.C., Morikawa, Y., Leach, J.P., Heallen, T., Cao, S., Krijger,
931 P.H.L., de Laat, W., Wehrens, X.H.T., Rodney, G.G., et al. (2019). YAP partially
932 reprograms chromatin accessibility to directly induce adult cardiogenesis in vivo. Dev.
933 Cell *48*, 765-779.e7. 10.1016/j.devcel.2019.01.017.

934 38. Cordenonsi, M., Zanconato, F., Azzolin, L., Forcato, M., Rosato, A., Frasson, C., Inui,
935 M., Montagner, M., Parenti, A.R., Poletti, A., et al. (2011). The Hippo transducer TAZ
936 confers cancer stem cell-related traits on breast cancer cells. Cell *147*, 759–772.
937 10.1016/j.cell.2011.09.048.

938 39. Xie, Q., Chen, J., Feng, H., Peng, S., Adams, U., Bai, Y., Huang, L., Li, J., Huang, J.,
939 Meng, S., et al. (2013). YAP/TEAD-mediated transcription controls cellular senescence.
940 Cancer Res. *73*, 3615–3624. 10.1158/0008-5472.CAN-12-3793.

941 40. Zhang, S., Chen, Q., Liu, Q., Li, Y., Sun, X., Hong, L., Ji, S., Liu, C., Geng, J., Zhang,
942 W., et al. (2017). Hippo Signaling Suppresses Cell Ploidy and Tumorigenesis through
943 Skp2. Cancer Cell *31*, 669-684.e7. 10.1016/j.ccell.2017.04.004.

944 41. Koo, J.H., Plouffe, S.W., Meng, Z., Lee, D.-H., Yang, D., Lim, D.-S., Wang, C.-Y., and
945 Guan, K.-L. (2020). Induction of AP-1 by YAP/TAZ contributes to cell proliferation and
946 organ growth. Genes Dev. *34*, 72–86. 10.1101/gad.331546.119.

947 42. Kim, M., Kim, T., Johnson, R.L., and Lim, D.-S. (2015). Transcriptional co-repressor
948 function of the hippo pathway transducers YAP and TAZ. Cell Rep. *11*, 270–282.
949 10.1016/j.celrep.2015.03.015.

950 43. Diehl, J.A., Cheng, M., Roussel, M.F., and Sherr, C.J. (1998). Glycogen synthase kinase-
951 3beta regulates cyclin D1 proteolysis and subcellular localization. Genes Dev. *12*, 3499–
952 3511. 10.1101/gad.12.22.3499.

953 44. Malek, N.P., Sundberg, H., McGrew, S., Nakayama, K., Kyriakides, T.R., and Roberts,
954 J.M. (2001). A mouse knock-in model exposes sequential proteolytic pathways that
955 regulate p27Kip1 in G1 and S phase. Nature *413*, 323–327. 10.1038/35095083.

956 45. Spencer, S.L., Cappell, S.D., Tsai, F.-C., Overton, K.W., Wang, C.L., and Meyer, T.
957 (2013). The proliferation-quiescence decision is controlled by a bifurcation in CDK2
958 activity at mitotic exit. Cell *155*, 369–383. 10.1016/j.cell.2013.08.062.

959 46. Shao, D.D., Xue, W., Krall, E.B., Bhutkar, A., Piccioni, F., Wang, X., Schinzel, A.C.,
960 Sood, S., Rosenbluh, J., Kim, J.W., et al. (2014). KRAS and YAP1 converge to regulate
961 EMT and tumor survival. Cell *158*, 171–184. 10.1016/j.cell.2014.06.004.

962 47. Wang, X., Freire Valls, A., Schermann, G., Shen, Y., Moya, I.M., Castro, L., Urban, S.,
963 Solecki, G.M., Winkler, F., Riedemann, L., et al. (2017). YAP/TAZ Orchestrate VEGF
964 Signaling during Developmental Angiogenesis. Dev. Cell *42*, 462-478.e7.
965 10.1016/j.devcel.2017.08.002.

966 48. Komuro, A., Nagai, M., Navin, N.E., and Sudol, M. (2003). WW domain-containing
967 protein YAP associates with ErbB-4 and acts as a co-transcriptional activator for the
968 carboxyl-terminal fragment of ErbB-4 that translocates to the nucleus. J. Biol. Chem. *278*,
969 33334–33341. 10.1074/jbc.M305597200.

970 49. He, C., Lv, X., Hua, G., Lele, S.M., Remmenga, S., Dong, J., Davis, J.S., and Wang, C.
971 (2015). YAP forms autocrine loops with the ERBB pathway to regulate ovarian cancer
972 initiation and progression. Oncogene *34*, 6040–6054. 10.1038/onc.2015.52.

973 50. Yuan, Y., Park, J., Feng, A., Awasthi, P., Wang, Z., Chen, Q., and Iglesias-Bartolome, R.
974 (2020). YAP1/TAZ-TEAD transcriptional networks maintain skin homeostasis by
975 regulating cell proliferation and limiting KLF4 activity. Nat. Commun. *11*, 1472.
976 10.1038/s41467-020-15301-0.

977 51. King, B., Araki, J., Palm, W., and Thompson, C.B. (2020). Yap/Taz promote the
978 scavenging of extracellular nutrients through macropinocytosis. Genes Dev. *34*, 1345–
979 1358. 10.1101/gad.340661.120.

980 52. Gillies, T.E., Pargett, M., Minguet, M., Davies, A.E., and Albeck, J.G. (2017). Linear
981 Integration of ERK Activity Predominates over Persistence Detection in Fra-1
982 Regulation. Cell Syst. *5*, 549-563.e5. 10.1016/j.cels.2017.10.019.

983 53. Edwards, A.C., Stalnecker, C.A., Jean Morales, A., Taylor, K.E., Klomp, J.E., Klomp,
984 J.A., Waters, A.M., Sudhakar, N., Hallin, J., Tang, T.T., et al. (2023). TEAD Inhibition
985 Overcomes YAP1/TAZ-Driven Primary and Acquired Resistance to KRASG12C
986 Inhibitors. Cancer Res. *83*, 4112–4129. 10.1158/0008-5472.CAN-23-2994.

987 54. Vaidyanathan, S., Salmi, T.M., Sathiqu, R.M., McConville, M.J., Cox, A.G., and Brown,
988 K.K. (2022). YAP regulates an SGK1/mTORC1/SREBP-dependent lipogenic program to
989 support proliferation and tissue growth. Dev. Cell *57*, 719-731.e8.
990 10.1016/j.devcel.2022.02.004.

991 55. Tumaneng, K., Schlegelmilch, K., Russell, R.C., Yimlamai, D., Basnet, H., Mahadevan,
992 N., Fitamant, J., Bardeesy, N., Camargo, F.D., and Guan, K.-L. (2012). YAP mediates
993 crosstalk between the Hippo and PI(3)K–TOR pathways by suppressing PTEN via miR-
994 29. Nat. Cell Biol. *14*, 1322–1329. 10.1038/ncb2615.

995 56. Zoncu, R., Efeyan, A., and Sabatini, D.M. (2011). mTOR: from growth signal integration
996 to cancer, diabetes and ageing. Nat. Rev. Mol. Cell Biol. *12*, 21–35. 10.1038/nrm3025.

997 57. Averous, J., Fonseca, B.D., and Proud, C.G. (2008). Regulation of cyclin D1 expression
998 by mTORC1 signaling requires eukaryotic initiation factor 4E-binding protein 1.
999 Oncogene *27*, 1106–1113. 10.1038/sj.onc.1210715.

1000 58. Hamaratoglu, F., Willecke, M., Kango-Singh, M., Nolo, R., Hyun, E., Tao, C., Jafar-
1001 Nejad, H., and Halder, G. (2006). The tumour-suppressor genes NF2/Merlin and

1002 Expanded act through Hippo signalling to regulate cell proliferation and apoptosis. Nat.
1003 Cell Biol. *8*, 27–36. 10.1038/ncb1339.

1004 59. Striedinger, K., VandenBerg, S.R., Baia, G.S., McDermott, M.W., Gutmann, D.H., and
1005 Lal, A. (2008). The neurofibromatosis 2 tumor suppressor gene product, merlin, regulates
1006 human meningioma cell growth by signaling through YAP. Neoplasia *10*, 1204–1212.
1007 10.1593/neo.08642.

1008 60. Yin, F., Yu, J., Zheng, Y., Chen, Q., Zhang, N., and Pan, D. (2013). Spatial organization
1009 of Hippo signaling at the plasma membrane mediated by the tumor suppressor
1010 Merlin/NF2. Cell *154*, 1342–1355. 10.1016/j.cell.2013.08.025.

1011 61. Wada, K.-I., Itoga, K., Okano, T., Yonemura, S., and Sasaki, H. (2011). Hippo pathway
1012 regulation by cell morphology and stress fibers. Development *138*, 3907–3914.
1013 10.1242/dev.070987.

1014 62. Aragona, M., Panciera, T., Manfrin, A., Giulitti, S., Michielin, F., Elvassore, N., Dupont,
1015 S., and Piccolo, S. (2013). A mechanical checkpoint controls multicellular growth
1016 through YAP/TAZ regulation by actin-processing factors. Cell *154*, 1047–1059.
1017 10.1016/j.cell.2013.07.042.

1018 63. Ong, Y.T., Andrade, J., Armbruster, M., Shi, C., Castro, M., Costa, A.S.H., Sugino, T.,
1019 Eelen, G., Zimmermann, B., Wilhelm, K., et al. (2022). A YAP/TAZ-TEAD signalling
1020 module links endothelial nutrient acquisition to angiogenic growth. Nat. Metab. *4*, 672–
1021 682. 10.1038/s42255-022-00584-y.

1022 64. Su, T., Bondar, T., Zhou, X., Zhang, C., He, H., and Medzhitov, R. (2015). Two-signal
1023 requirement for growth-promoting function of Yap in hepatocytes. eLife *4*.
1024 10.7554/eLife.02948.

1025 65. Chen, Q., Zhang, N., Xie, R., Wang, W., Cai, J., Choi, K.-S., David, K.K., Huang, B.,
1026 Yabuta, N., Nojima, H., et al. (2015). Homeostatic control of Hippo signaling activity
1027 revealed by an endogenous activating mutation in YAP. Genes Dev. *29*, 1285–1297.
1028 10.1101/gad.264234.115.

1029 66. Meyer, K., Lammers, N.C., Bugaj, L.J., Garcia, H.G., and Weiner, O.D. (2023).
1030 Optogenetic control of YAP reveals a dynamic communication code for stem cell fate and
1031 proliferation. Nat. Commun. *14*, 6929. 10.1038/s41467-023-42643-2.

1032 67. Franklin, J.M., Ghosh, R.P., Shi, Q., Reddick, M.P., and Liphardt, J.T. (2020). Concerted
1033 localization-resets precede YAP-dependent transcription. Nat. Commun. *11*, 4581.
1034 10.1038/s41467-020-18368-x.

1035 68. Manning, S.A., Dent, L.G., Kondo, S., Zhao, Z.W., Plachta, N., and Harvey, K.F. (2018).
1036 Dynamic fluctuations in subcellular localization of the hippo pathway effector yorkie
1037 in vivo. Curr. Biol. *28*, 1651-1660.e4. 10.1016/j.cub.2018.04.018.

1038 69. Curto, M., Cole, B.K., Lallemand, D., Liu, C.-H., and McClatchey, A.I. (2007). Contact-
1039 dependent inhibition of EGFR signaling by Nf2/Merlin. J. Cell Biol. *177*, 893–903.
1040 10.1083/jcb.200703010.

1041 70. Moleirinho, S., Hoxha, S., Mandati, V., Curtale, G., Troutman, S., Ehmer, U., and Kissil,
1042 J.L. (2017). Regulation of localization and function of the transcriptional co-activator
1043 YAP by angiomotin. eLife *6*. 10.7554/eLife.23966.

1044 71. Yi, C., Troutman, S., Fera, D., Stemmer-Rachamimov, A., Avila, J.L., Christian, N.,
1045 Persson, N.L., Shimono, A., Speicher, D.W., Marmorstein, R., et al. (2011). A tight
1046 junction-associated Merlin-angiomotin complex mediates Merlin's regulation of
1047 mitogenic signaling and tumor suppressive functions. Cancer Cell *19*, 527–540.
1048 10.1016/j.ccr.2011.02.017.

1049 72. Kapoor, A., Yao, W., Ying, H., Hua, S., Liewen, A., Wang, Q., Zhong, Y., Wu, C.-J.,
1050 Sadanandam, A., Hu, B., et al. (2014). Yap1 activation enables bypass of oncogenic Kras
1051 addiction in pancreatic cancer. Cell *158*, 185–197. 10.1016/j.cell.2014.06.003.

1052 73. Jang, W., Kim, T., Koo, J.S., Kim, S.-K., and Lim, D.-S. (2017). Mechanical cue-induced
1053 YAP instructs Skp2-dependent cell cycle exit and oncogenic signaling. EMBO J. *36*,
1054 2510–2528. 10.15252/embj.201696089.

1055 74. Kossatz, U., Dietrich, N., Zender, L., Buer, J., Manns, M.P., and Malek, N.P. (2004).
1056 Skp2-dependent degradation of p27kip1 is essential for cell cycle progression. Genes
1057 Dev. *18*, 2602–2607. 10.1101/gad.321004.

1058 75. Adachi, Y., Kimura, R., Hirade, K., Yanase, S., Nishioka, Y., Kasuga, N., Yamaguchi,
1059 R., and Ebi, H. (2023). Scribble mis-localization induces adaptive resistance to KRAS
1060 G12C inhibitors through feedback activation of MAPK signaling mediated by YAP-
1061 induced MRAS. Nat. Cancer *4*, 829–843. 10.1038/s43018-023-00575-2.

1062 76. Lin, L., Sabnis, A.J., Chan, E., Olivas, V., Cade, L., Pazarentzos, E., Asthana, S., Neel,
1063 D., Yan, J.J., Lu, X., et al. (2015). The Hippo effector YAP promotes resistance to RAF-
1064 and MEK-targeted cancer therapies. Nat. Genet. *47*, 250–256. 10.1038/ng.3218.

1065 77. Ratnayeke, N., Baris, Y., Chung, M., Yeeles, J.T.P., and Meyer, T. (2023). CDT1 inhibits
1066 CMG helicase in early S phase to separate origin licensing from DNA synthesis. Mol.
1067 Cell *83*, 26-42.e13. 10.1016/j.molcel.2022.12.004.

1068 78. Ran, F.A., Hsu, P.D., Wright, J., Agarwala, V., Scott, D.A., and Zhang, F. (2013).
1069 Genome engineering using the CRISPR-Cas9 system. Nat. Protoc. *8*, 2281–2308.
1070 10.1038/nprot.2013.143.

1071 79. Sakaue-Sawano, A., Kurokawa, H., Morimura, T., Hanyu, A., Hama, H., Osawa, H.,
1072 Kashiwagi, S., Fukami, K., Miyata, T., Miyoshi, H., et al. (2008). Visualizing

1073 spatiotemporal dynamics of multicellular cell-cycle progression. Cell *132*, 487–498.
1074 10.1016/j.cell.2007.12.033.

1075 80. Schindelin, J., Arganda-Carreras, I., Frise, E., Kaynig, V., Longair, M., Pietzsch, T.,
1076 Preibisch, S., Rueden, C., Saalfeld, S., Schmid, B., et al. (2012). Fiji: an open-source
1077 platform for biological-image analysis. Nat. Methods *9*, 676–682. 10.1038/nmeth.2019.

1078 81. Stallaert, W., Kedziora, K.M., Taylor, C.D., Zikry, T.M., Ranek, J.S., Sobon, H.K.,
1079 Taylor, S.R., Young, C.L., Cook, J.G., and Purvis, J.E. (2022). The structure of the
1080 human cell cycle. Cell Syst. *13*, 230-240.e3. 10.1016/j.cels.2021.10.007.

1081 82. Kim, D., Paggi, J.M., Park, C., Bennett, C., and Salzberg, S.L. (2019). Graph-based
1082 genome alignment and genotyping with HISAT2 and HISAT-genotype. Nat. Biotechnol.
1083 *37*, 907–915. 10.1038/s41587-019-0201-4.

1084 83. Liao, Y., Smyth, G.K., and Shi, W. (2014). featureCounts: an efficient general purpose
1085 program for assigning sequence reads to genomic features. Bioinformatics *30*, 923–930.
1086 10.1093/bioinformatics/btt656.

1087 84. Love, M.I., Huber, W., and Anders, S. (2014). Moderated estimation of fold change and
1088 dispersion for RNA-seq data with DESeq2. Genome Biol. *15*, 550. 10.1186/s13059-014-
1089 0550-8.

1090

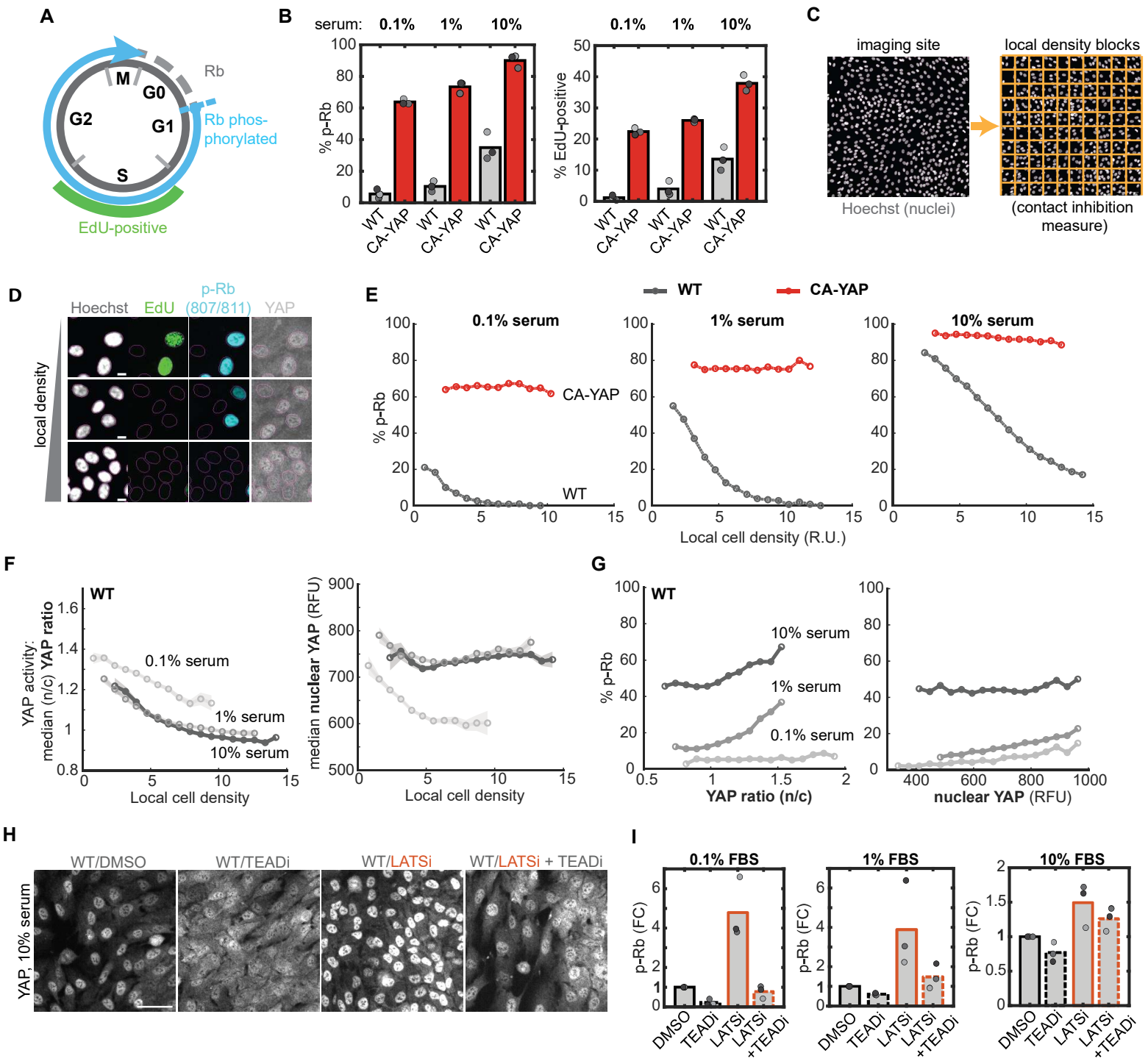

Figure 1. Contact inhibition of YAP opposes mitogen stimulation in a balance mechanism that controls proliferation

1091 **Figure 1. Contact inhibition of YAP opposes mitogen stimulation in a balance mechanism**
1092 **that controls proliferation**
1093
1094 **A)** Diagram of cell cycle phases: EdU incorporation marks S-phase, Rb hyperphosphorylation
1095 (p-Rb, S807/811) cycling cells.
1096 **B)** Mean percent p-Rb (left) and EdU-positive (right) for wild-type (WT) and CA-YAP cells
1097 maintained in increasing serum levels (0.1%, 1%, or 10%) for 36h. N = 3 independent
1098 experiments. Student's t-test (p-Rb, EdU): p= 6.86×10^{-6}, 1.01×10^{-5} (0.1% serum), p= 2.50×10^{-5},
1099 8.13×10^{-5} (1% serum), p= 5.90×10^{-4}, 7.13×10^{-4} (10% serum).
1100 **C)** Representation of local cell density metric, by subdividing imaging sites into 10x10 grids and
1101 counting the cells (by centroid of segmented nucleus) for each block (see also Methods, scale
1102 bar = 100 μm).
1103 **D)** Sample images of RPE1 cells at increasing local cell density: Hoechst for DNA (white), EdU
1104 for S-phase cells (green), p-Rb for cycling cells (blue), and YAP (grey). Magenta outline is the
1105 automated nuclear mask (scale bar = 10 μm).
1106 **E)** Percent p-Rb binned by local density for WT and CA-YAP treated as in (B). The percent was
1107 calculated as the fraction of p-Rb-positive cells from cells binned by the local cell density metric
1108 (relative units, R.U.), n > 20,000 cells/condition. See also **Figure S1**.
1109 **F)** Median nuclear/cytoplasmic (n/c) YAP ratio (left) and nuclear YAP levels (right, real
1110 fluorescent units, RFU) per local density bin for WT cells treated as in (C), n > 20,000
1111 cells/condition. Shaded error bars are 95% confidence intervals.
1112 **G)** Percent p-Rb for WT cells binned by their YAP ratio (left) or nuclear YAP levels (right) for
1113 cells treated as in (C).
1114 **H**) Representative images of YAP staining for WT cells treated with TEAD inhibitor (TEADi, 0.5
1115 μM GNE-7883), LATS inhibitor (LATSi, 0.5 μM TDI-011536) or in combination in 10% serum for
1116 24h.
1117 **I)** Fold-change in percent p-Rb for WT cells treated with TEADi, LATSi, or in combination,
1118 normalized to DMSO in 0.1% (left), 1% (middle), or 10% serum (right). N = 3 independent
1119 experiments.
1120 All binned plots have n>100 cells/bin and >20,000 cells/condition.

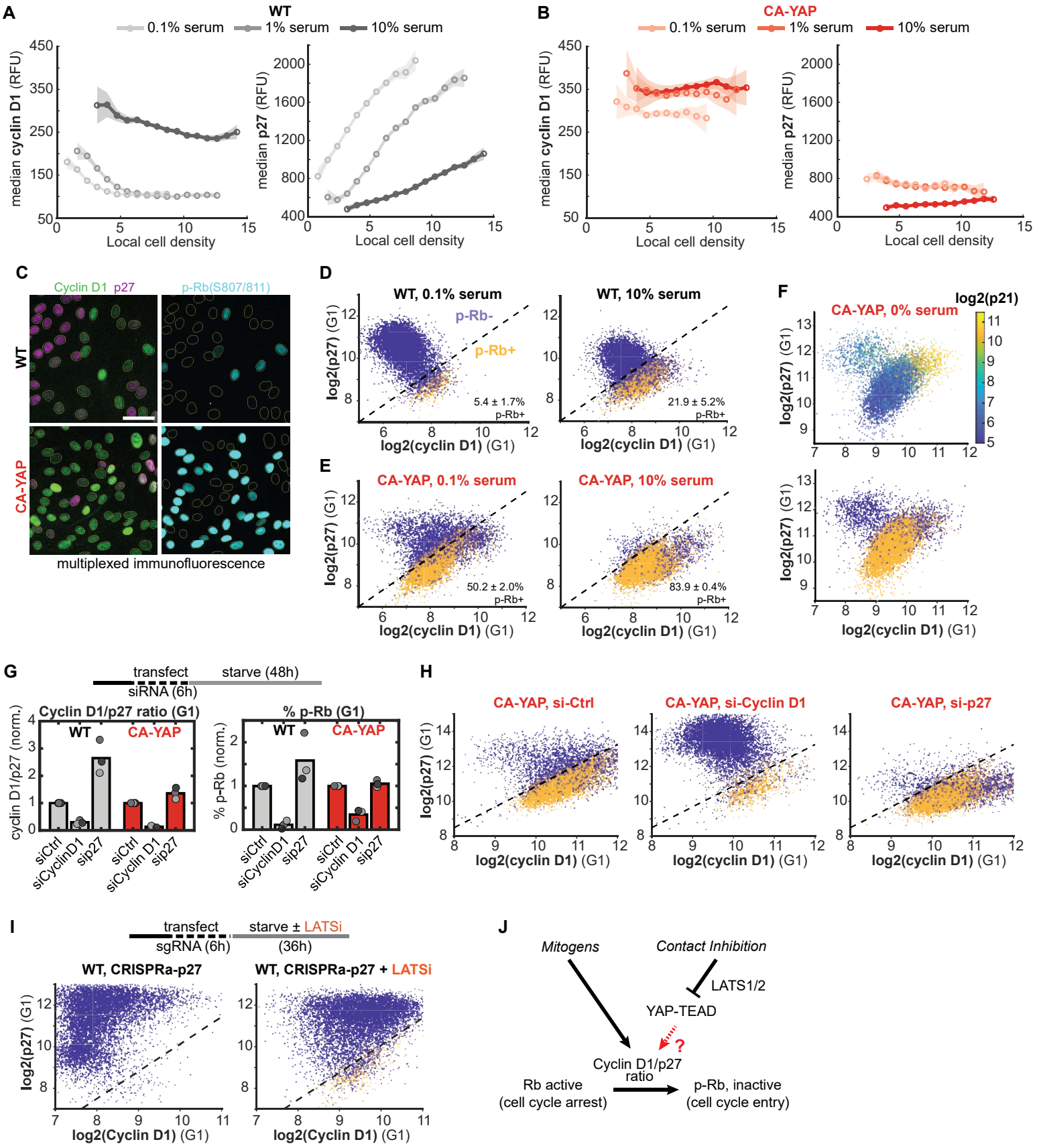

Figure 2. YAP-regulated cell cycle entry and exit is dictated by the cyclin D1/p27 threshold

1121 **Figure 2. YAP-regulated cell cycle entry and exit is dictated by the cyclin D1/p27**
1122 **threshold**
1123
1124 **A-B)** Median levels (real fluorescent units (RFU)) of cyclin D1 (left) and p27 (right) per local cell
1125 density bin for WT (A) and CA-YAP (B) cells at 0.1%, 1%, and 10% serum. Binned data only
1126 include G1-gated cells, n > 100 cells/bin. Shaded error bars are 95% confidence intervals, n >
1127 15,000 cells per condition. Data are representative of 2 independent experiments.
1128 **C**) Representative images of multiplexed immunofluorescence staining comparing cyclin D1
1129 (green) and p27 levels (magenta) with aligned p-Rb stain (cyan, with gray nuclear mask overlay)
1130 in WT or CA-YAP cells. Scale bar = 50 µm.
1131 **D-E**) Representative single-cell scatterplots of co-stained cyclin D1 and p27 levels (log2-
1132 transformed), colored by p-Rb (purple, p-Rb-negative; orange, p-Rb-positive) in WT (D) and CA-
1133 YAP (E). Left, 0.1% serum; right, 10% serum. Mean ± SD of 2 independent experiments.
1134 **F**) Representative single-cell scatterplots of serum-starved CA-YAP cells co-stained for cyclin
1135 D1 and p27 protein levels, colored by p21 protein levels (top: parula color scale) or p-Rb status
1136 (bottom: purple, p-Rb-negative; orange, p-Rb-positive).
1137 **G**) Top: experimental conditions for siRNA transfection followed by 48h serum starvation.
1138 Bottom: mean cyclin D1/p27 ratio (left) and p-Rb (right) for WT and CA-YAP cells transfected
1139 with siRNA against cyclin D1 and p27, normalized to non-targeting control (siCtrl). N = 3
1140 independent experiments.
1141 **H**) Representative single-cell scatterplots of co-stained cyclin D1 and p27 levels colored by p-
1142 Rb for CA-YAP cells treated as in (G).
1143 **I)** Top: experimental conditions for sgRNA-mediated overexpression (CRISPRa) of p27 in
1144 dCas9-expressing WT cells treated with DMSO or LATSi (0.5 µM TDI-011536). Bottom:
1145 Representative single-cell scatterplots of co-stained cyclin D1 and p27 levels colored by p-Rb
1146 for p27-overexpressing cells treated with DMSO (left) or LATSi (right).
1147 **J**) Schematic of mitogen signaling and contact inhibition of YAP-TEAD activity converging on
1148 the cyclin D1/p27 ratio to control whether cells enter or exit the cell cycle.
1149 Dashed lines approximate separation of p-Rb-positive and p-Rb-negative cell populations.
1150 Single-cell data are representative of 2 independent experiments, with n = 8,000 random
1151 cells/scatter plot and gated for G1-phase (defined as 2N DNA/EdU-negative status). See also
1152 **Figure S2**.
1153

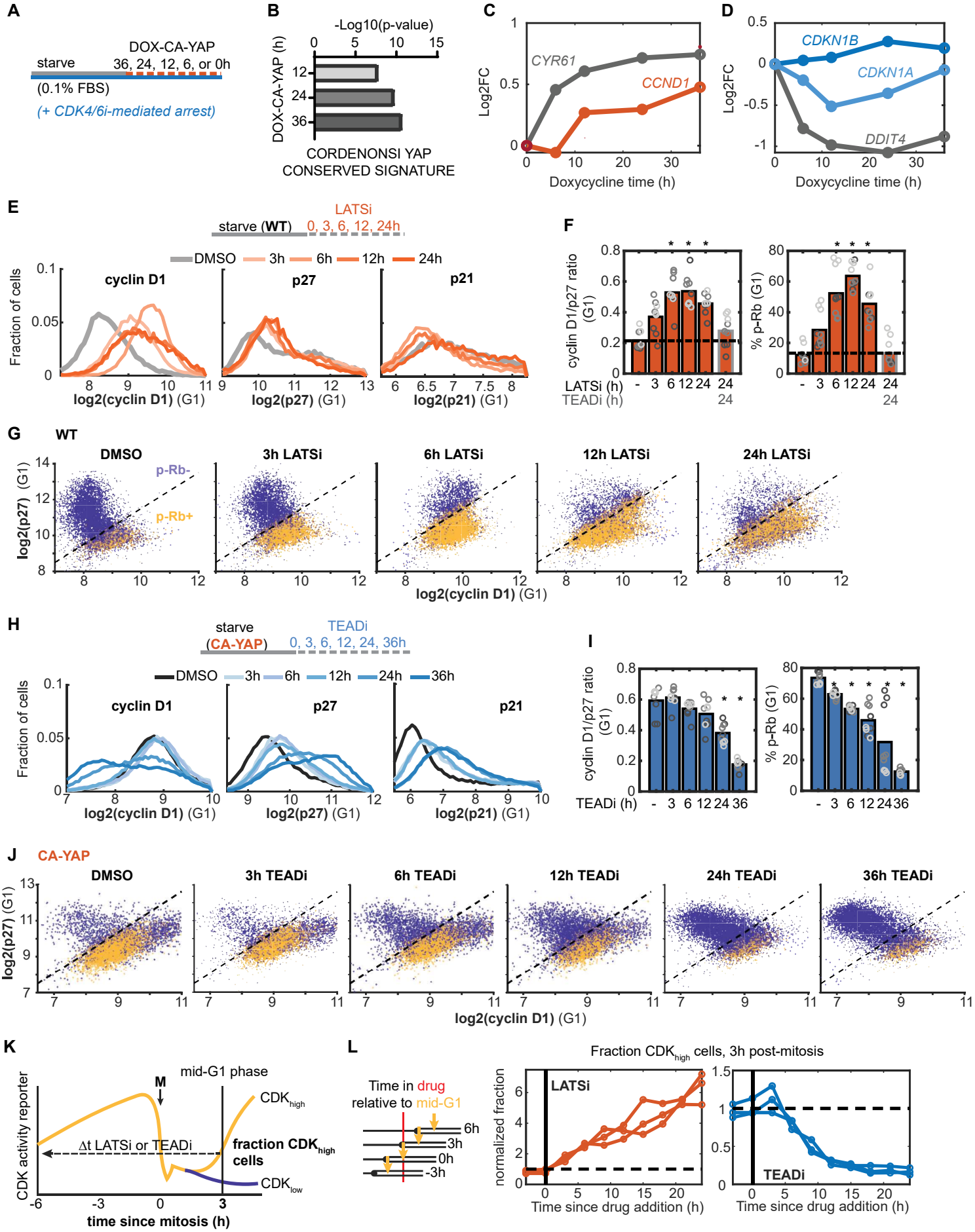

Figure 3. Delayed YAP-mediated control of the cyclin D1/p27 ratio and cell cycle arrest

1154 **Figure 3. Delayed YAP-mediated control of the cyclin D1/p27 ratio and cell cycle arrest**
1155
1156 **A)** Schematic for CA-YAP expression in RPE1 cells. RNA-sequencing performed in confluent
1157 cells pre-conditioned at 0.1% and palbociclib-arrested (CDK4/6i, 1 μM), prior to doxycycline-
1158 induction over 36h (0.5 μg/mL DOX). See also **Figure S3** and Methods.
1159 **B)** Up-regulated genes ($q<0.05$, Log2 fold-change >1) for 12, 24, and 36h YAP induction
1160 showed the Cordenonsi YAP signature (using ToppGene)[38].
1161 **C-D)** Log2 fold-change (Log2FC) induction (C) of *CYR61* (canonical YAP target gene, grey)
1162 compared with *CCND1* (cyclin D1, red) and (D) regulation of DDIT4 (suppressed YAP target
1163 gene, grey), *CDKN1A* (p21, dark blue), and *CDKN1B* (p27, blue) at times since
1164 overexpression. Adjusted p-values (NS at all other time points): *CCND1*, 3.17×10^{-4} (12h), 4.45
1165 $\times 10^{-5}$ (24h), 3.96×10^{-12} (36h); *CDKN1A*, 8.65×10^{-7} (12h), 9.5×10^{-4} (24h); *CDKN1B*, 0.0012 (24h),
1166 0.0312 (36h).
1167 **E)** Top: Experimental conditions for LATSi treatment (0.5 μM TDI-011536) of serum-starved WT
1168 cells for 0-24h. Bottom: Histogram distribution of cyclin D1, p27, and p21 protein levels over
1169 LATSi time course.
1170 **F)** Mean cyclin D1/p27 ratio (left) and percent p-Rb (right) for cells treated as in (E). N = 3
1171 independent experiments and 3 well-replicates/experiment, as indicated by matched
1172 colors. Student's t-test: cyclin D1/p27, $p = 0.0062$ (6h), 0.0022 (12h), 2.63×10^{-4} (24h); p-Rb, $p =$
1173 0.0217 (6h), 4.12×10^{-4} (12h), 0.0087 (24h).
1174 **G)** Representative single-cell scatterplots of cyclin D1 and p27 protein levels colored by p-Rb
1175 status (purple, p-Rb-negative; orange, p-Rb-positive).
1176 **H)** Top: experimental conditions for TEADi treatment (1 μM GNE-7883) of serum-starved CA-
1177 YAP cells. Bottom: Histogram distribution of cyclin D1, p27, and p21 protein levels over TEADi
1178 time course.
1179 **I)** Mean cyclin D1/p27 ratio (left) and percent p-Rb (right) for cells treated as in (H). N = 3
1180 biological replicates, where well-replicates are indicated by matched colors. Student's t-test:
1181 cyclin D1/p27 ratio, $p = 0.027$ (24h), $p = 0.0015$ (36h); % p-Rb, $p = 0.0188$ (3h), $p = 0.0011$ (6h),
1182 0.0119 (12h), $p = 0.0481$ (24h), $p = 1.98 \times 10^{-5}$ (36h).
1183 **J)** Representative single-cell scatterplots of cyclin D1 and p27 protein levels colored by p-Rb
1184 status for cells treated as in (H).
1185 **K)** Schematic for bifurcation of the CDK2 activity reporter for asynchronously cycling cells
1186 computationally aligned by mitosis and analysis of CDK_{high} fraction for cells born after variable
1187 time in DMSO, LATSi, or TEADi treatment (see also Methods).
1188 **L)** Schematic representing variable time cells experienced drug relative to mitosis and 3h post-
1189 mitosis (mid-G1 indicator, left) and normalized fraction of CDK_{high} cells at 3h post-mitosis,
1190 binned by time spent in LATSi or TEADi (right). The fraction of CDK_{high} cells was normalized to
1191 the DMSO control treatment (n = 3 independent experiments, n > 5,000 cells/condition).
1192 All histogram and single-cell data (n = 8,000 cells/scatterplot) are representative of 3
1193 independent experiments.
1194

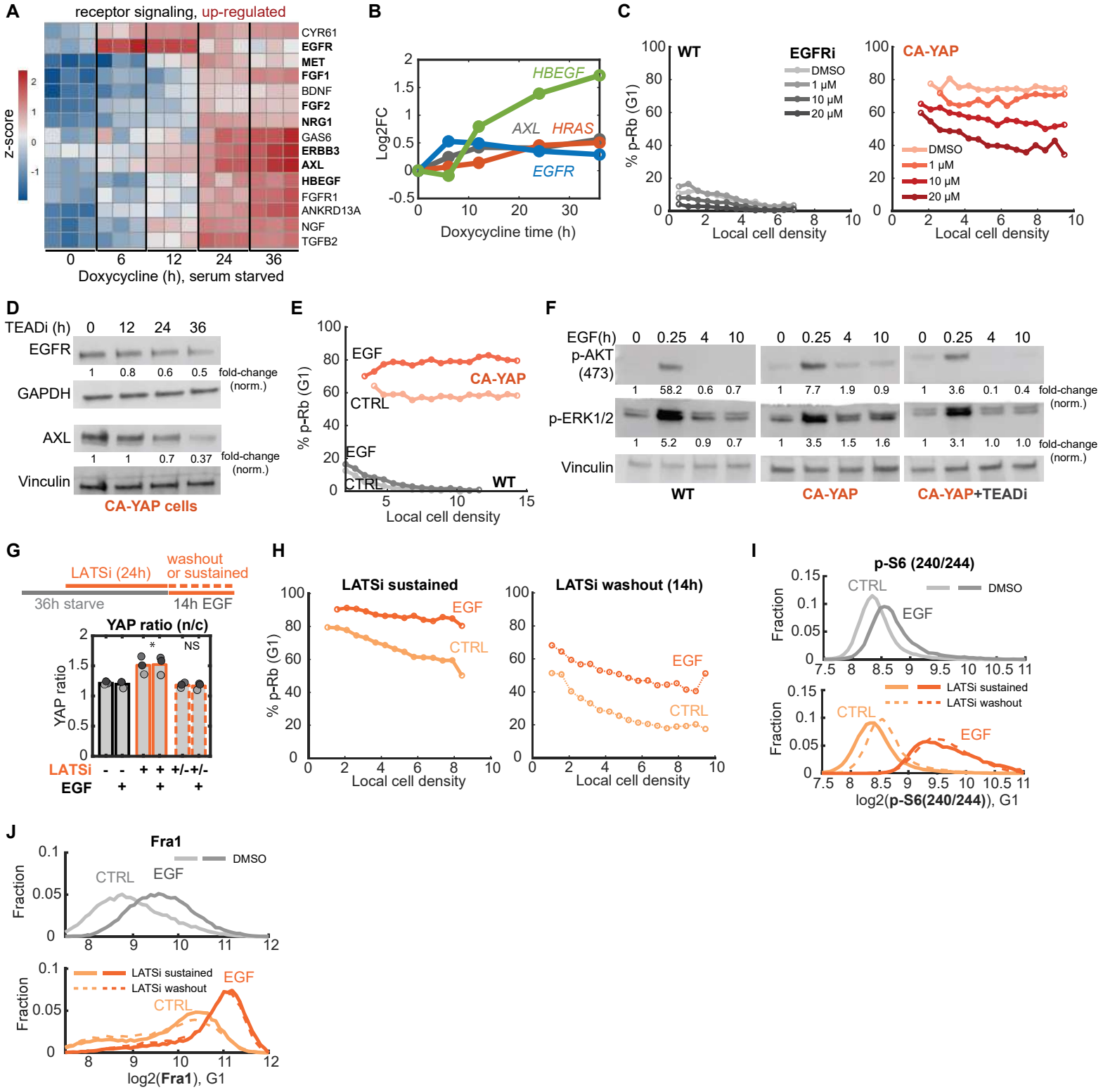

Figure 4. YAP activation induces and prolongs proliferation by increasing EGFR signaling

1195 **Figure 4. YAP activation induces and prolongs proliferation by increasing EGFR**
1196 **signaling**
1197
1198 **A)** Heatmap representation of differential expression (row z-score) of select up-regulated ligand
1199 and receptor genes, grouped by 3 independent replicates and time points.
1200 **B)** Log2 fold-change (Log2FC) of select receptor signaling-related genes, *AXL* (direct YAP
1201 target, grey), *EGFR* (blue), *HBEGF* (green), and *HRAS* (red). Adjusted p-values: *AXL,* 6.20
1202 $x10^{-4}$ (6h), $9.11x10^{-12}$ (12h), $2.33x10^{-11}$(24h), $2.19x10^{-21}$ (36h); *EGFR,* $4.97x10^{-16}$ (6h), $1.07x10^{-14}$
1203 (12h), $1.07x10^{-8}$ (24h), $1.23x10^{-5}$ (36h); *HBEGF*, $3.90x10^{-4}$ (12h), $8.57x10^{-12}$ (24h), $5.24x10^{-18}$
1204 (36h); *HRAS*, $4.10x10^{-4}$ (24h), $6.05x10^{-5}$ (36h).
1205 **C)** Percent p-Rb binned by local cell density for WT (left) and CA-YAP (right) cells serum-
1206 starved and treated with gefitinib (EGFRi, 0-20 μM) for 24h. See also **Figure S4.**
1207 **D)** Western blot analysis of EGFR and AXL from whole-cell lysates of serum-starved CA-YAP
1208 cells treated with TEADi for 0-36h, with GAPDH and Vinculin loading controls. Values indicate
1209 fold-change difference relative to 0h control (after normalization to loading control). Data are
1210 representative of 2 independent experiments.
1211 **E)** Percent p-Rb binned by local density for serum-starved WT and CA-YAP cells after 14h EGF
1212 (25 ng/mL). Data are representative of 2 independent experiments, n > 25,000 cells/condition.
1213 **F)** Western blot analysis of AKT and ERK phosphorylation levels in whole-cell lysates of serum-
1214 starved WT (left), CA-YAP (middle), and TEADi pre-treated CA-YAP cells (right) after 0-10h
1215 EGF treatment (25 ng/mL). Values indicate fold-change difference relative to 0h control (after
1216 normalization to loading control).
1217 **G)** Top: experimental conditions for serum-starvation of WT cells, pre-treatment with LATSi, and
1218 sustained or washout of LATSi during 14h EGF treatment (25 ng/mL). Bottom: Mean YAP ratio
1219 (n/c) for treatment conditions. N = 3 independent experiments, matched colors indicate
1220 conditions from the same experimental replicate. Student's t-test to control, YAP ratio: LATSi
1221 sustained, p= 0.0278 (CTRL), 0.027 (EGF); LATSi washout, not significant (NS).
1222 **H)** Percent p-Rb binned by local cell density for cells with LATSi sustained (left) or washout
1223 (right) with or without EGF treatment, n > 20,000 cells/condition.
1224 **I-J)** Histogram distribution of phosphorylated-S6 (p-S6 240/244, I) and Fra1 protein levels for
1225 DMSO-treated (top, CTRL) or LATSi-pretreated cells (bottom, LATSi sustained and washout).
1226 Data are representative of 3 independent experiments.
1227 All single-cell data represent values from G1-gated cells.
1228

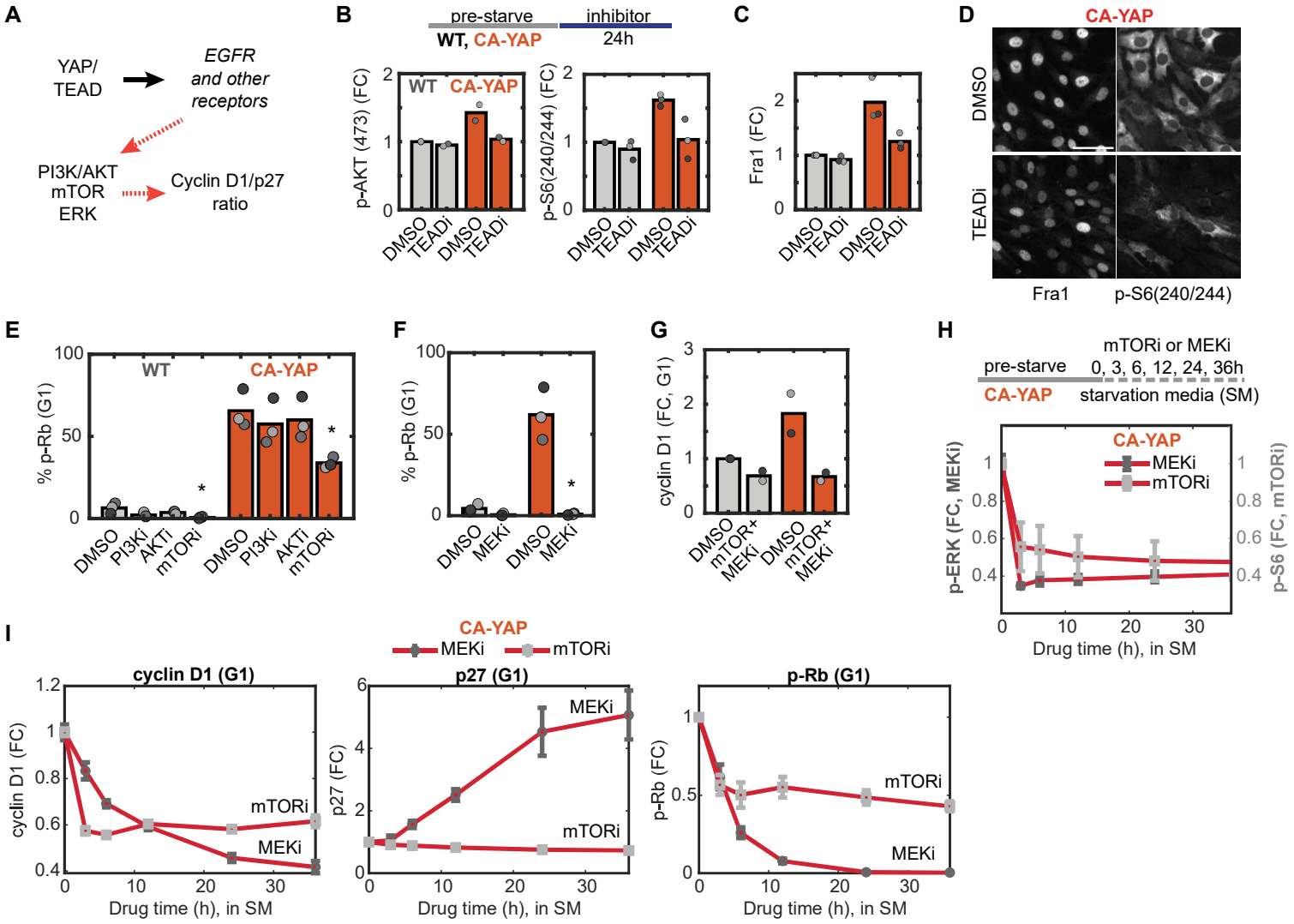

Figure 5. YAP activation signals through ERK and mTOR to increase the cyclin D1/p27 ratio

1229 **Figure 5. YAP activation signals through ERK and mTOR to increase the cyclin D1/p27**
1230 **ratio**
1231
1232 **A)** Schematic of proposed indirect regulation of cyclin D1/p27 ratio by YAP/TEAD via EGFR-
1233 activated signaling pathways.
1234 **B-C)** Top: experimental conditions for serum-starvation of WT and CA-YAP cells followed by
1235 24h treatment with TEAD inhibitor for 24h in starvation media. Bottom: Mean fold-change (FC)
1236 in protein levels of p-AKT(473, left) and p-S6(240/244, right) (B) and Fra1 (C) for serum-starved
1237 WT and CA-YAP cells treated with TEADi for 24h (normalized to WT/DMSO condition). N = 2
1238 (p-AKT) or n = 3 (p-S6, Fra1) independent experiments.
1239 **D)** Representative multiplexed images for Fra1 and p-S6(240/244) staining in CA-YAP cells
1240 treated with TEADi as in (B). Scale bar = 50 μm.
1241 **E-F)** Mean percentage p-Rb for WT and CA-YAP cells treated with PI3K (LY294002, 10 μM),
1242 AKT (MK2206, 200 nM), or mTORC1/2 (Torin2, 100 nM) inhibitors (E) or MEK (PD0325901,
1243 100 nM) inhibitor (F) as in (B). N = 3 independent experiments. Student's t-test: WT/mTORi, p =
1244 0.0372; CA-YAP/mTORi, p = 0.0103 (E). CA-YAP/MEKi, p = 0.0028 (F). See also **Figure S5**.
1245 **G)** Mean FC in cyclin D1 protein levels for WT and CA-YAP cells treated with combined mTORi
1246 and MEKi relative to WT/DMSO condition as in (B). N = 2 independent experiments.
1247 **H)** Top: experiment conditions for mTORi or MEKi time course treatment of serum-starved CA-
1248 YAP cells. Bottom: fold-change in p-ERK (MEKi-treated, dark grey) and p-S6(240/244, mTORi-
1249 treated, light grey) following drug treatment. Mean ± SEM (n = 2 independent experiments, 2-3
1250 replicate wells/experiment).
1251 **I)** Fold-change in protein levels of cyclin D1, p27, and p-Rb for MEKi and mTORi for CA-YAP
1252 cells treated as in (H). Mean ± SEM.
1253

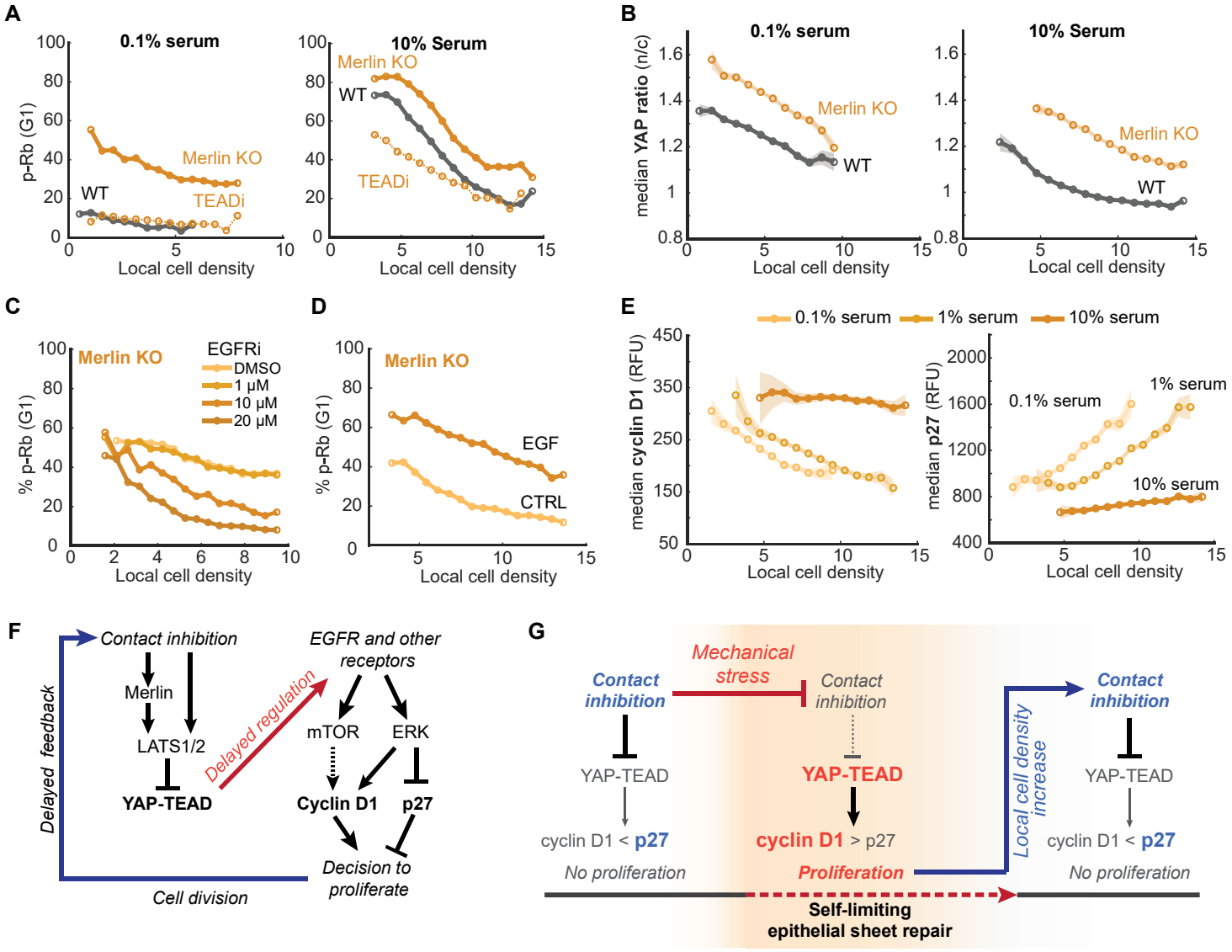

Figure 6. Partial activation of YAP by Merlin knockout can be reversed by increased contact inhibition

1254 **Figure 6. Partial activation of YAP by Merlin knockout can be reversed by increased**
1255 **contact inhibition**
1256
1257 **A)** TEAD-dependent hyperproliferation of Merlin KO cells. Percent p-Rb binned by local density
1258 for Merlin knockout cells (Merlin KO, yellow) in 0.1% (left) or 10% serum (right) treated with
1259 DMSO or TEADi (0.5 μM) compared with WT cells (grey).
1260 **B)** Median YAP ratio (n/c) binned by local cell density for Merlin KO cells in 0.1% (left) or 10%
1261 serum (right), compared with WT cells (same experiment as in **Figure 1E**). Data are
1262 representative of 3 independent experiments. Shaded error are 95% confidence intervals.
1263 **C)** Percent p-Rb binned by local density for serum-starved Merlin KO cells treated with gefitinib
1264 (EGFRi). Data are representative of 2 independent experiments.
1265 **D)** Percent p-Rb binned by local cell density for serum-starved Merlin KO cells with control
1266 (CTRL) or EGF (25 ng/mL) treatment for 12h. Data are representative of 2 independent
1267 experiments.
1268 **E)** Median cyclin D1 (left) or p27 (right) protein levels for Merlin KO cells in titrated serum.
1269 Shaded error are 95% confidence intervals. Data are representative of 2 independent
1270 experiments.
1271 **F)** Model for Hippo-pathway inhibition of YAP-TEAD activity, which regulates signaling through
1272 and downstream of EGFR to control the cyclin D1/p27 ratio.
1273 **G)** Model proposing transitions between low and high YAP-TEAD activity as contact inhibition is
1274 temporarily reduced then recovered after a delay during epithelial sheet regeneration.
1275 For all representative binned plots, data are pooled from at least 2 wells, n > 100 cells/bin, n >
1276 10,000 cells/plot. All quantifications are for G1-gated cells. See also **Figure S6**.
1277

Figure S1

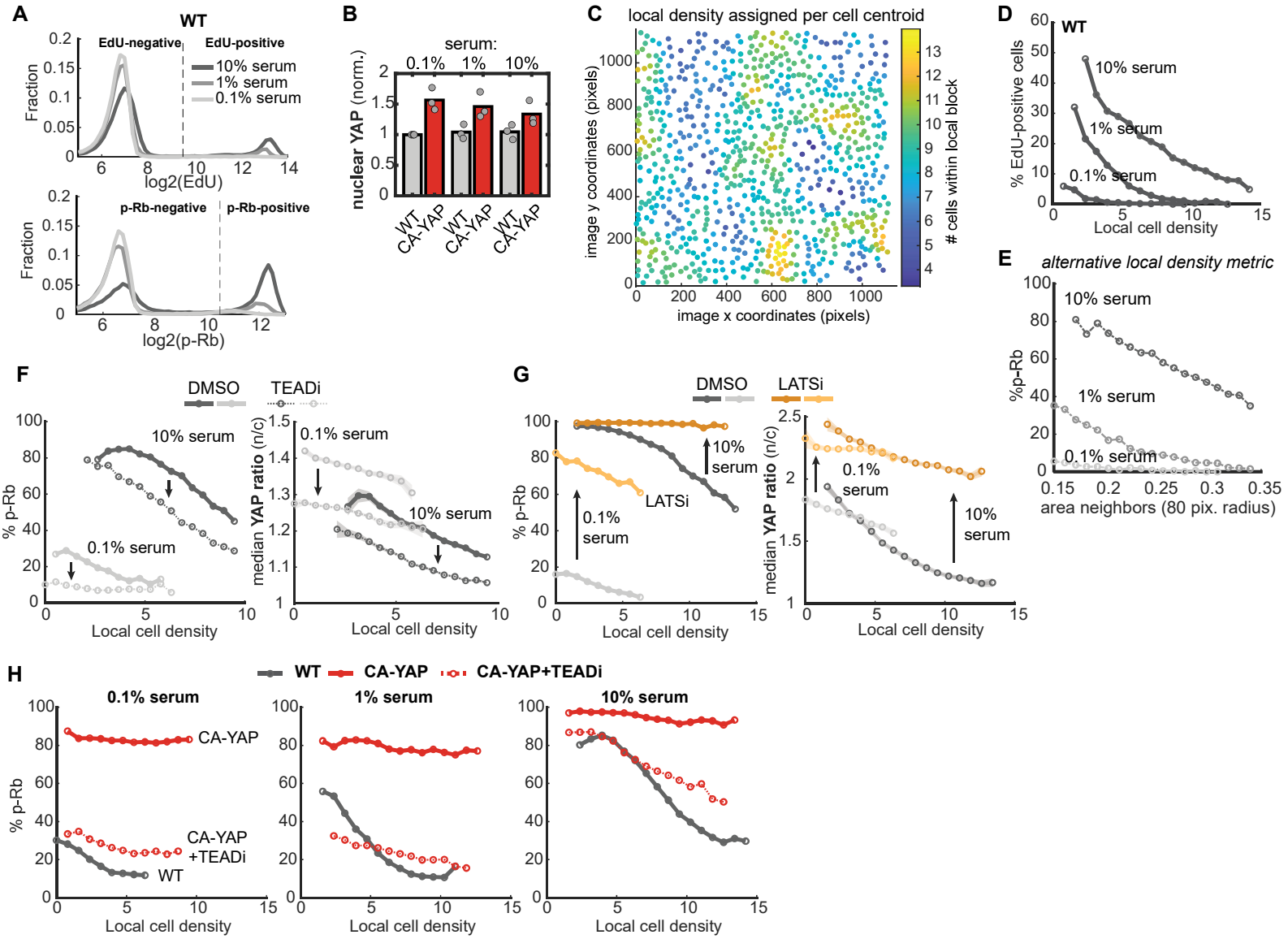
A
WT
EdU-negative
EdU-positive
10% serum
1% serum
0.1% serum
Fraction
log2(EdU)
p-Rb-negative
p-Rb-positive
log2(p-Rb)
B
serum:
0.1%
1%
10%
nuclear YAP (norm.)
WT
CA-YAP
C
local density assigned per cell centroid
image y coordinates (pixels)
image x coordinates (pixels)
cells within local block
D
WT
% EdU-positive cells
10% serum
1% serum
0.1% serum
Local cell density
E
alternative local density metric
%p-Rb
area neighbors (80 pix. radius)
F
DMSO
TEADi
% p-Rb
median YAP ratio (n/c)
Local cell density
G
DMSO
LATSi
LATSi
H
WT
CA-YAP
CA-YAP+TEADi
0.1% serum
1% serum
10% serum
% p-Rb
Local cell density

1278 **Figure S1, related to Figure 1**
1279
1280 **A)** Histogram plots of binary distribution of EdU (top) and Rb phosphorylation (phospho-Rb
1281 807/811, bottom) in WT RPE1 cells with 10%, 1%, or 0.1% serum. Dashed line indicates cutoff
1282 values used to designed whether cells are EdU-positive or have phosphorylated Rb. Data are
1283 representative of 3 independent experiments (same experiment as in Figure 1E).
1284 **B)** Mean nuclear YAP protein levels in serum-titrated WT and CA-YAP cells, normalized (norm.)
1285 to WT/0.1% serum condition for each experiment, n = 3 independent experiments.
1286 **C)** Representative local density estimation in an imaging site, where circles represent the
1287 location of the centroids of cell nuclei. Cell location coordinates were divided into a 10x10,
1288 equally-spaced grid (local density blocks). The z-scale color indicates the number of cell
1289 centroids within a block. Cells were assigned local densities based on the number of cells in
1290 their block, scaled by the image size to give a relative density unit. See also Methods.
1291 **D)** Percent EdU-positive cells per local density bin for WT cells in titrated serum levels. Data are
1292 representative of 3 independent experiments.
1293 **E)** Percent p-Rb binned by alternate local density metric (area of neighboring cell nuclear pixels
1294 within an 80-pixel (~51.6 μm) radius) for WT cells in titrated serum, showing similar density
1295 dependence as the primary local density metric.
1296 **F-G)** Percent p-Rb (left) and median YAP ratio (nuclear/cytoplasmic, n/c, right) binned by local
1297 density for WT and CA-YAP cells in 0.1% and 10% serum. Cells were treated with DMSO and
1298 TEADi (1 μM GNE-7883, F, dashed lines) or LATSi (0.5 μM TDI-011536, G, orange lines) for
1299 24h. Shaded error are 95% confidence intervals, n > 15,000 cells/condition. Arrows highlight
1300 drug-mediated changes for matched serum conditions.
1301 **H)** Percent p-Rb per local density bin for WT (grey) and CA-YAP cells (red) treated with DMSO
1302 or TEADi (0.5 μM, dashed line) in titrated serum.
1303 All binned and histogram data are from one representative replicate of 3 independent
1304 experiments, n >100 cells/bin and n >15,000 cells/condition).
1305

Figure S2

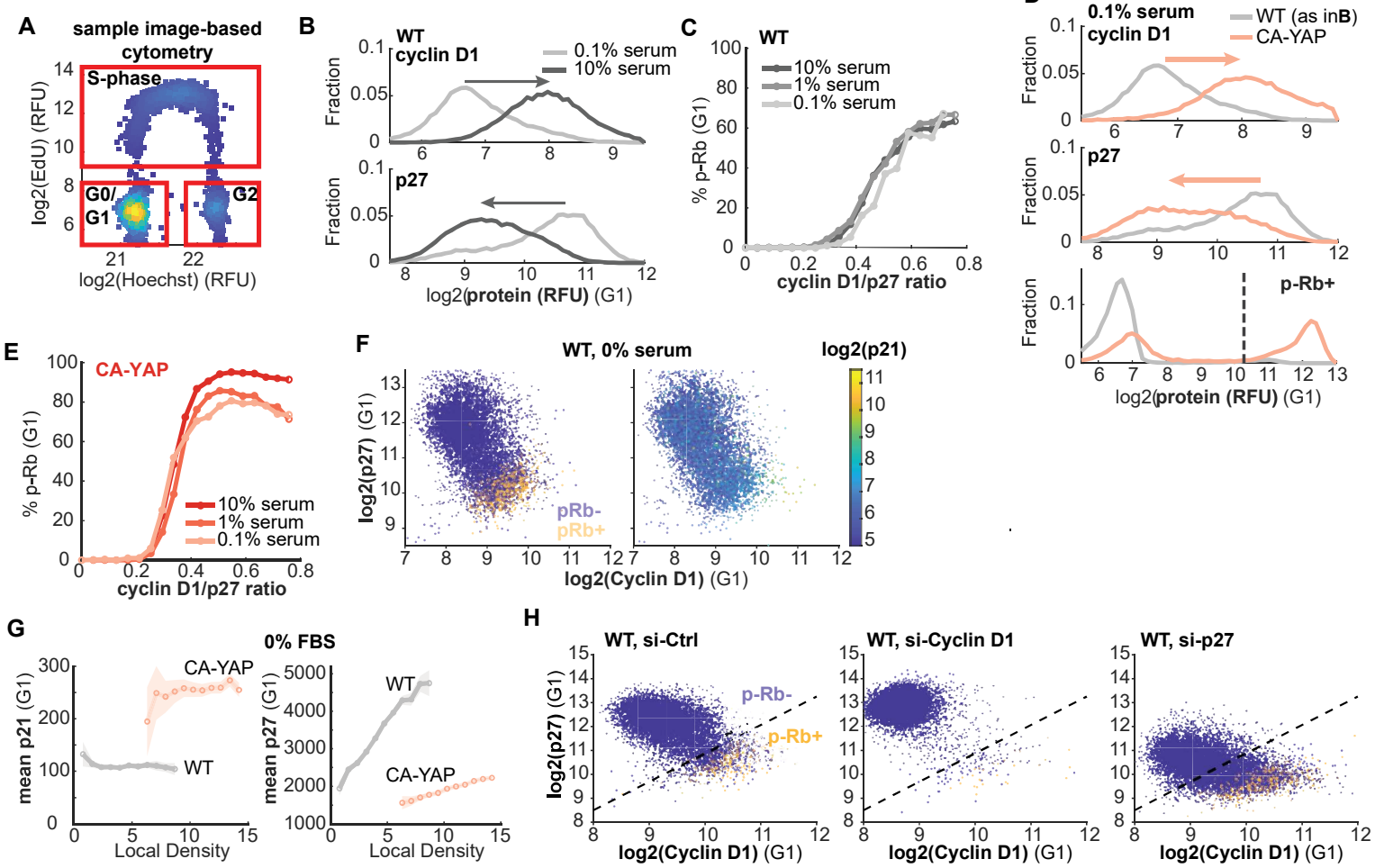
A
sample image-based cytometry
S-phase
G0/G1
G2
log2(EdU) (RFU)
log2(Hoechst) (RFU)
B
WT
cyclin D1
0.1% serum
10% serum
p27
Fraction
log2(protein (RFU) (G1)
C
WT
10% serum
1% serum
0.1% serum
% p-Rb (G1)
cyclin D1/p27 ratio
D
0.1% serum
cyclin D1
WT (as in B)
CA-YAP
p27
p-Rb+
Fraction
log2(protein (RFU) (G1)
E
CA-YAP
10% serum
1% serum
0.1% serum
% p-Rb (G1)
cyclin D1/p27 ratio
F
WT, 0% serum
log2(p21)
pRb-
pRb+
log2(p27) (G1)
log2(Cyclin D1) (G1)
G
0% FBS
CA-YAP
WT
mean p21 (G1)
mean p27 (G1)
Local Density
H
WT, si-Ctrl
WT, si-Cyclin D1
WT, si-p27
p-Rb-
p-Rb+
log2(p27) (G1)
log2(Cyclin D1) (G1)

1306 **Figure S2, related to Figure 2**
1307
1308 **A)** Representative density scatterplot of DNA content (Hoechst staining, real fluorescence units
1309 (RFU)) and EdU-incorporation for G0/G1 gating of cells. G1 population cells were defined as 2N
1310 DNA/EdU-negative, S-cells as EdU-positive, and G2 as 4N DNA/EdU-negative. All-cell gating
1311 reflects cells within the outer red boundary (n = 8,000 random cells).
1312 **B)** Histogram distribution of cyclin D1 protein (top) and p27 protein (bottom) stain in WT cells in
1313 0.1% or 10% FBS.
1314 **C)** Percent p-Rb binned by cyclin D1/p27 ratio for serum titration in WT cells (n > 15,000
1315 cells/condition).
1316 **D)** Histogram distribution of cyclin D1 (top), p27 (middle), and p-Rb (bottom) stain comparing
1317 CA-YAP cells with WT in 0.1% FBS (same WT data as S1A), n > 20,000 cells/condition. Dashed
1318 line indicates p-Rb cutoff.
1319 **E)** Percent p-Rb binned by cyclin D1/p27 ratio for serum titration in CA-YAP cells (n > 15,000
1320 cells/condition).
1321 **F)** Representative density scatterplot of cyclin D1 stain against p27 stain, colored by binary p-
1322 Rb status (left) or p21 stain (right, parula scale) in starved WT cells.
1323 **G)** Mean p21 (left) and p27 (right) protein levels (RFU) binned by local density for starved WT
1324 (grey), and CA-YAP (red) cells (n > 20,000 cells/condition). Shaded error are 95% confidence
1325 intervals.
1326 **H)** Representative density scatterplots of cyclin D1 and p27 protein levels (RFU) colored by p-
1327 Rb status for serum-starved WT cells transfected with siRNA against control (si-Ctrl, left), cyclin
1328 D1 (si-Cyclin D1, middle), or p27 (si-p27, right). Dashed, diagonal line visually approximates
1329 where p-Rb bifurcates in CA-YAP conditions (matching Figure 2H).
1330 All data representative of 2 independent experiments and gated for G1-phase. All single-cell
1331 scatterplots show n = 8,000 cells.
1332

Figure S3

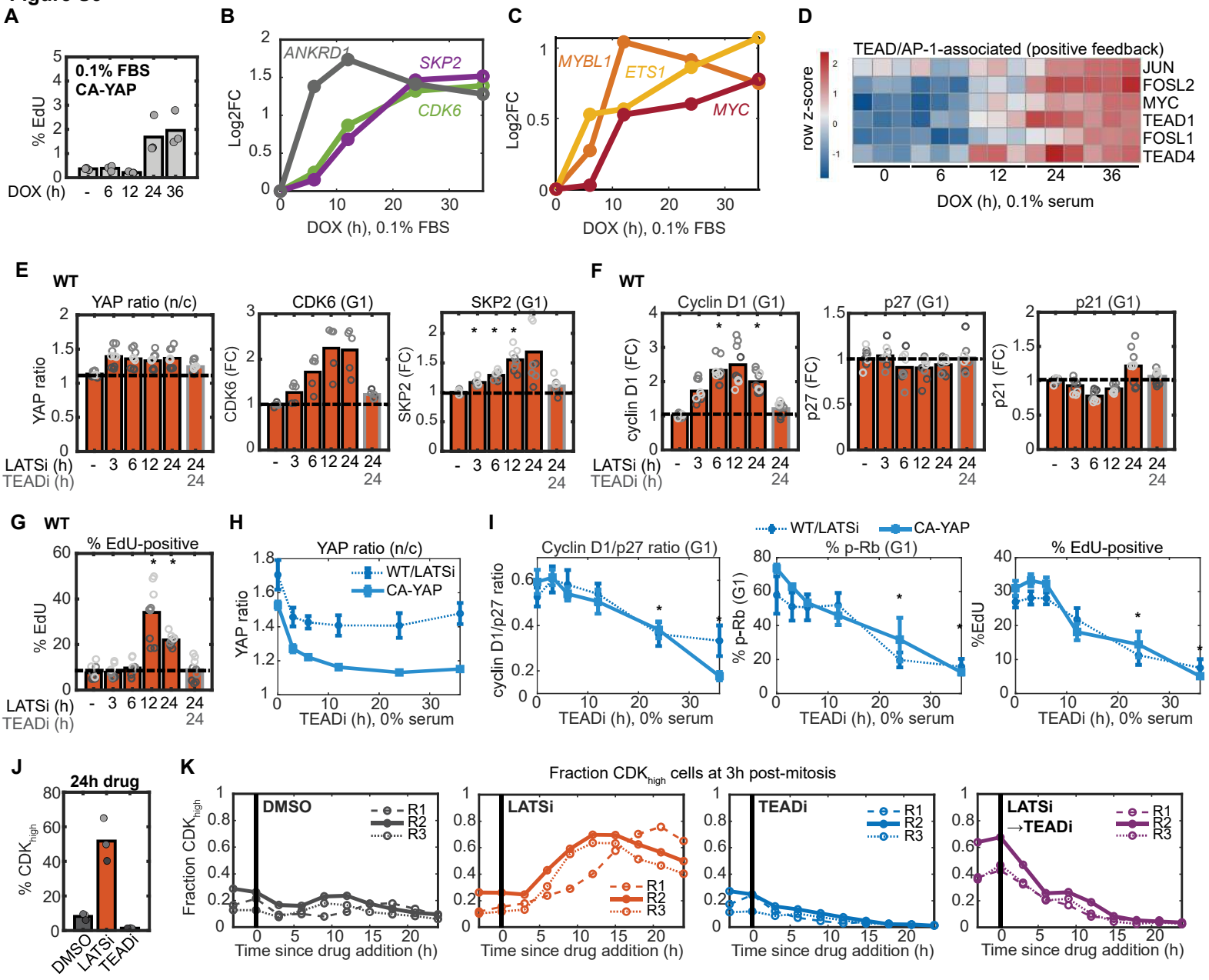
A
0.1% FBS
CA-YAP
% EdU
DOX (h)
- 6 12 24 36
B
ANKRD1
SKP2
CDK6
Log2FC
DOX (h), 0.1% FBS
C
MYBL1
ETS1
MYC
Log2FC
DOX (h), 0.1% FBS
D
TEAD/AP-1-associated (positive feedback)
row z-score
JUN
FOSL2
MYC
TEAD1
FOSL1
TEAD4
DOX (h), 0.1% serum
E
WT
YAP ratio (n/c)
CDK6 (G1)
SKP2 (G1)
YAP ratio
CDK6 (FC)
SKP2 (FC)
LATSi (h)
TEADi (h)
F
WT
Cyclin D1 (G1)
p27 (G1)
p21 (G1)
cyclin D1 (FC)
p27 (FC)
p21 (FC)
LATSi (h)
TEADi (h)
G
WT
% EdU-positive
% EdU
LATSi (h)
TEADi (h)
H
YAP ratio (n/c)
WT/LATSi
CA-YAP
YAP ratio
TEADi (h), 0% serum
I
WT/LATSi
CA-YAP
Cyclin D1/p27 ratio (G1)
% p-Rb (G1)
% EdU-positive
cyclin D1/p27 ratio
% p-Rb (G1)
%EdU
TEADi (h), 0% serum
J
24h drug
% CDKhigh
DMSO
LATSi
TEADi
K
Fraction CDKhigh cells at 3h post-mitosis
DMSO
LATSi
TEADi
LATSi →TEADi
R1
R2
R3
Fraction CDKhigh
Time since drug addition (h)

1333 **Figure S3, related to Figure 3**
1334
1335 **A)** Mean percent EdU for matched replicates of Figure 3A reserved for immunofluorescence
1336 staining for CA-YAP cells in 0.1% FBS and arrested with palbociclib (1μM) during treatment with
1337 DMSO (-) or doxycycline (DOX) for 0-36h. N = 3 independent experiments.
1338 **B-C)** Kinetics of sample YAP target gene induction. Log2 fold-change (Log2FC) induction of
1339 ANKRD1 (canonical YAP target gene, grey) compared with *CDK6* (green) and *SKP2* (purple)
1340 (B) and transcription factor targets *MYC* (red) compared with *MYBL1* (orange) and *ETS1*
1341 (yellow) at times since overexpression (C).
1342 Adjusted p-values: *CDK6*, 0.0451 (6h), 4.22 $x10^{-22}$ (12h), 3.08 $x10^{-52}$ (24h), 3.26 $x10^{-58}$ (36h);
1343 *SKP2*, 3.78 $x10^{-13}$ (12h), 3.49 $x10^{-65}$ (24h), 1.86 $x10^{-70}$ (36h); *MYC*, 2.18$x10^{-6}$(12h), 2.39$x10^{-8}$
1344 (24h), 1.50$x10^{-13}$ (36h); *MYBL1*, 7.77$x10^{-13}$ (12h), 2.76$x10^{-10}$ (24h), 3.48$x10^{-7}$ (36h); *ETS1*,
1345 1.85$x10^{-13}$ (6h), 4.55 $x10^{-16}$(12h), 6.24$x10^{-37}$(24h), 1.23$x10^{-57}$(36h).
1346 **D)** Heatmap of TEAD/AP-1-associated positive feedback genes in DOX-treated, CA-YAP cells.
1347 Color scale indicates row z-score.
1348 **E-G)** Mean YAP ratio (E, left) and fold-change in protein levels of CDK6 (E, middle), SKP2 (E,
1349 right), cyclin D1 (F, left), p27 (F, middle), p21 (F, right), and percent EdU (G) for serum starved,
1350 WT cells treated with LATSi (0.5 μM TDI-011536) for 0-24h or co-inhibited with TEADi (grey
1351 outline, 1 μM GNE-7883). N = 2 (CDK6) or 3 independent experiments (all other proteins).
1352 Student's one-sample t-test: SKP2, p = 0.0159 (3h), 0.0178 (6h), 0.0468 (12h); cyclin D1, p =
1353 0.0168 (6h), 0.0271 (24h); EdU, p = 0.0285 (12h), 6.65$x10^{-4}$ (24h).
1354 **H-I)** Mean YAP ratio (H), cyclin D1/p27 ratio (I, left), percent p-Rb (I, middle) and EdU-positive
1355 (I, right) cells following TEADi treatment of starved WT cells treated with LATSi (dashed line) or
1356 CA-YAP (solid line, same data as Figure 3I). Mean ± SEM (n = 3 independent experiments).
1357 Student's two-sample t-test, CA-YAP: cyclin D1/p27 ratio, p = 0.0354 (24h, 36h); %p-Rb, p =
1358 0.0377 (24h), 0.0328 (36h); EdU, 0.0038 (24h), 0.0012 (36h).
1359 **J)** Mean percentage CDK_{high} cells at 3h post-mitosis for cells reentering the cell cycle 24h after
1360 DMSO, LATSi, or TEADi treatment. N = 3 independent experiments.
1361 **K)** Fraction of CDK_{high} cells at 3h post-mitosis (mid-G1 phase) relative to drug treatment. Cells
1362 were aligned by mitosis and binned based on time spent in control (DMSO), LATSi, or TEADi (n
1363 > 100 cells/bin, n > 5,000 cells/condition). For the LATSi to TEADi drug change (right), cells
1364 were treated with LATSi for 12h prior to washout and treatment with TEADi. Each line
1365 represents an independent experiment (n = 3), where matched line styles indicate data from the
1366 same experiment.
1367 All fixed-cell data are G1-gated. Colored rings indicate replicate wells within matched
1368 experimental replicates.
1369

Figure S4

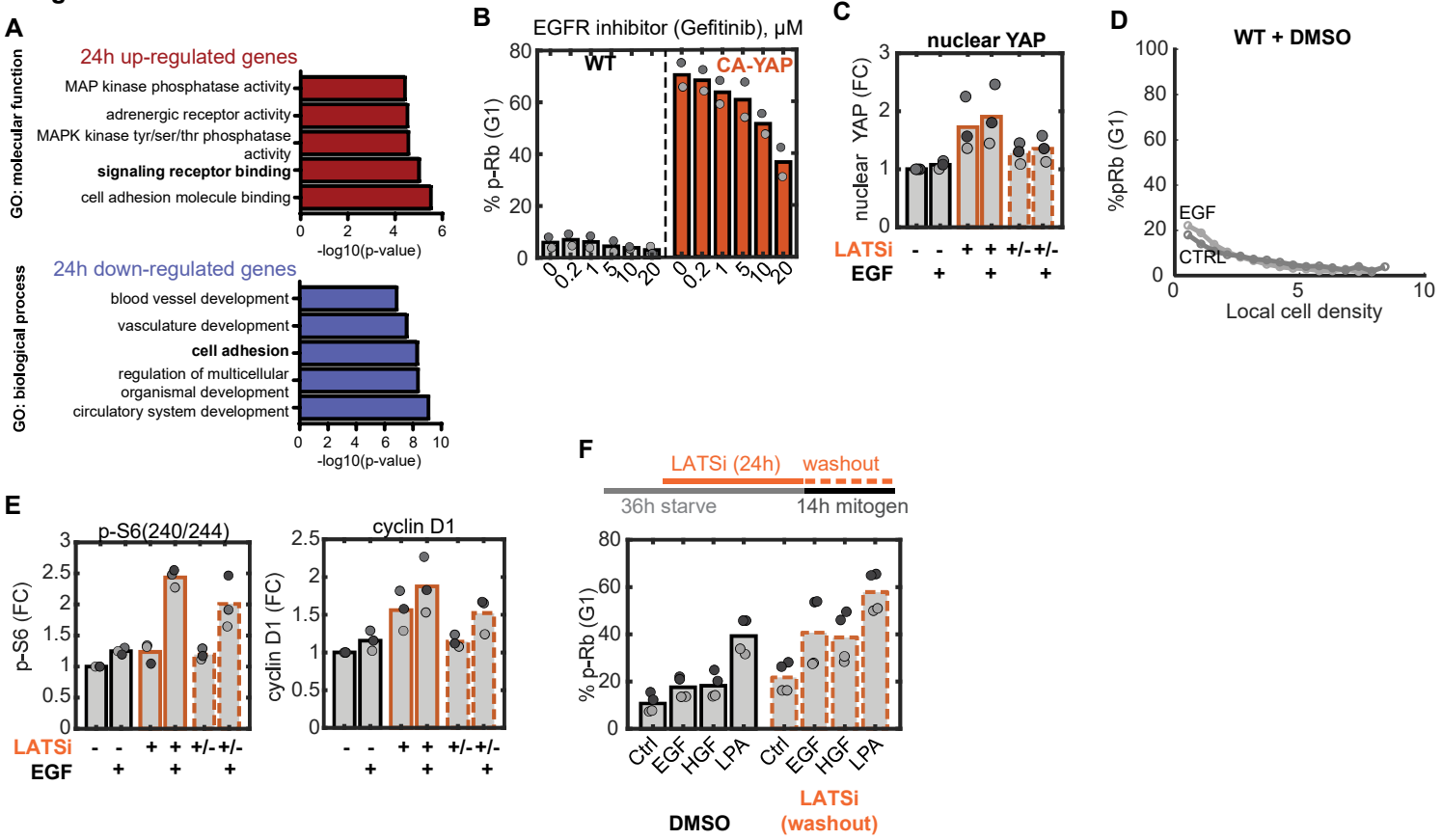
A
24h up-regulated genes
GO: molecular function
MAP kinase phosphatase activity
adrenergic receptor activity
MAPK kinase tyr/ser/thr phosphatase activity
signaling receptor binding
cell adhesion molecule binding
-log10(p-value)
24h down-regulated genes
GO: biological process
blood vessel development
vasculature development
cell adhesion
regulation of multicellular organismal development
circulatory system development
-log10(p-value)
B
EGFR inhibitor (Gefitinib), μM
WT
CA-YAP
% p-Rb (G1)
C
nuclear YAP
nuclear YAP (FC)
LATSi
EGF
D
WT + DMSO
%pRb (G1)
EGF
CTRL
Local cell density
E
p-S6(240/244)
p-S6 (FC)
cyclin D1
cyclin D1 (FC)
LATSi
EGF
F
LATSi (24h)
washout
36h starve
14h mitogen
% p-Rb (G1)
Ctrl
EGF
HGF
LPA
DMSO
LATSi (washout)

1370 **Figure S4, related to Figure 4**
1371
1372 **A)** Top: GO terms enriched for significantly up-regulated genes after 24-hour YAP induction ($q <$
1373 0.05, Log2FC > 1.0) relative to control (0.1 % FBS) (Figure 5A). Bottom: GO process terms
1374 enriched for significantly down-regulated genes ($q < 0.05$, Log2FC < -1.0).
1375 **B)** Mean percent p-Rb for serum-starved WT and CA-YAP cells treated with gefinitib (EGFR
1376 inhibitor) at indicated doses (μM) for 24h (n = 2 independent experiments).
1377 **C)** Mean fold-change in nuclear YAP levels for WT cells treated with DMSO or LATSi ± washout
1378 during EGF treatment (0.5 μM TDI-011536, 25 ng/mL EGF) as in Figure 4G (n = 3 independent
1379 experiments).
1380 **D)** Percent p-Rb binned by local density for serum-starved WT cells pre-treated with DMSO
1381 prior to 14h EGF (25 ng/mL) or control (CTRL) treatment, as in Figure 4G. Data are
1382 representative of 3 independent experiments (n > 25,000 cells/condition).
1383 **E)** Mean fold-change in cytoplasmic p-S6 (240/244, left) and cyclin D1 (right) for cells treated as
1384 in Figure 4G (n = 3 independent experiments, where matched colors indicate values from same
1385 experiment).
1386 **F)** Mean percent p-Rb for serum-starved WT cells pre-treated with DMSO or LATSi (5 μM,
1387 TRULI) for 24h prior to washout and 14h mitogen treatment (25 ng/mL EGF and HGF, 1 μM
1388 LPA). N = 2 independent experiments, where matched colors indicate well-
1389 replicates/experiment.
1390 All single-cell data are G1-gated cells.
1391
1392

Figure S5

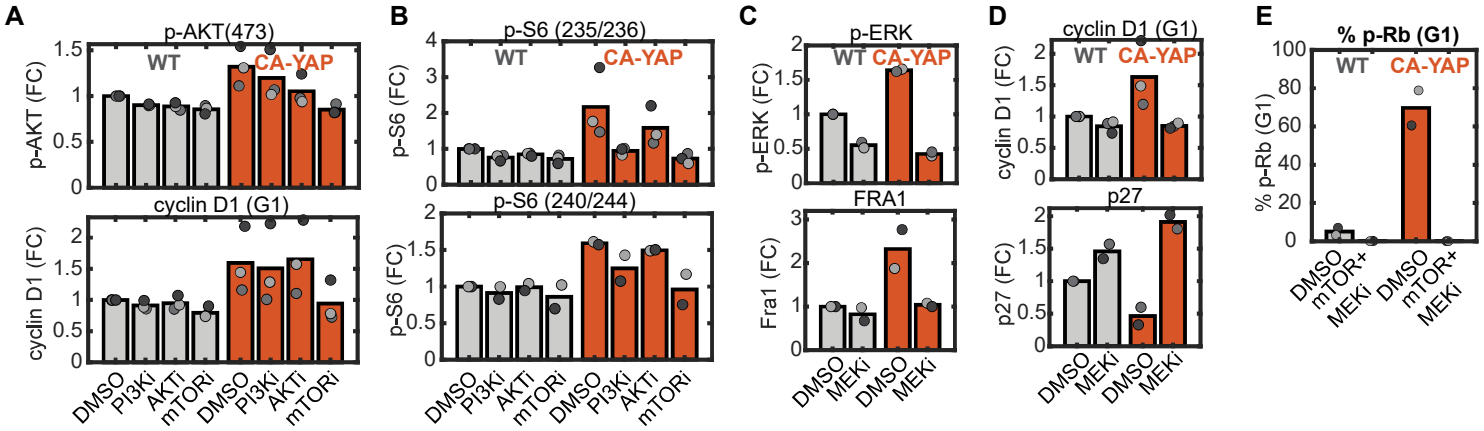
A
p-AKT(473)
WT
CA-YAP
p-AKT (FC)
cyclin D1 (G1)
cyclin D1 (FC)
DMSO
PI3Ki
AKTi
mTORi
B
p-S6 (235/236)
p-S6 (FC)
p-S6 (240/244)
C
p-ERK
p-ERK (FC)
FRA1
Fra1 (FC)
MEKi
D
cyclin D1 (G1)
cyclin D1 (FC)
p27
p27 (FC)
E
% p-Rb (G1)
% p-Rb (G1)
mTOR+
MEKi

1393 **Figure S5, related to Figure 5**
1394
1395 **A-B**) Fold-change in protein levels of p-AKT(S473) and cyclin D1 (A), and p-S6(B, top: 235/236;
1396 bottom: 240/244) for serum-starved WT and CA-YAP cells treated with PI3Ki, AKTi, or mTORi,
1397 as in Figure 5E. N = 2 (p-AKT, p-S6-240/244) or n = 3 (cyclin D1, p-S6-235/236) independent
1398 experiments, where matched colors indicate values from the same experiment.
1399 **C-D**) Mean fold-change in protein levels of p-ERK and Fra1 (C), cyclin D1 and p27 (D) for
1400 serum-starved WT and CA-YAP cells treated with MEKi as in Figure 5F. N = 2 (p-ERK, Fra1,
1401 p27) or n = 3 (cyclin D1) independent experiments, matched colors indicate values from the
1402 same experiment.
1403 **E**) Mean percent p-Rb in serum-starved WT and CA-YAP cells treated with DMSO or combined
1404 mTOR+MEKi (100 nM Torin2, 100 nM PD0325901). N = 2 independent experiments, matched
1405 colors indicate values from the same experiment.
1406 All data are from G1-gated cells.
1407

Figure S6

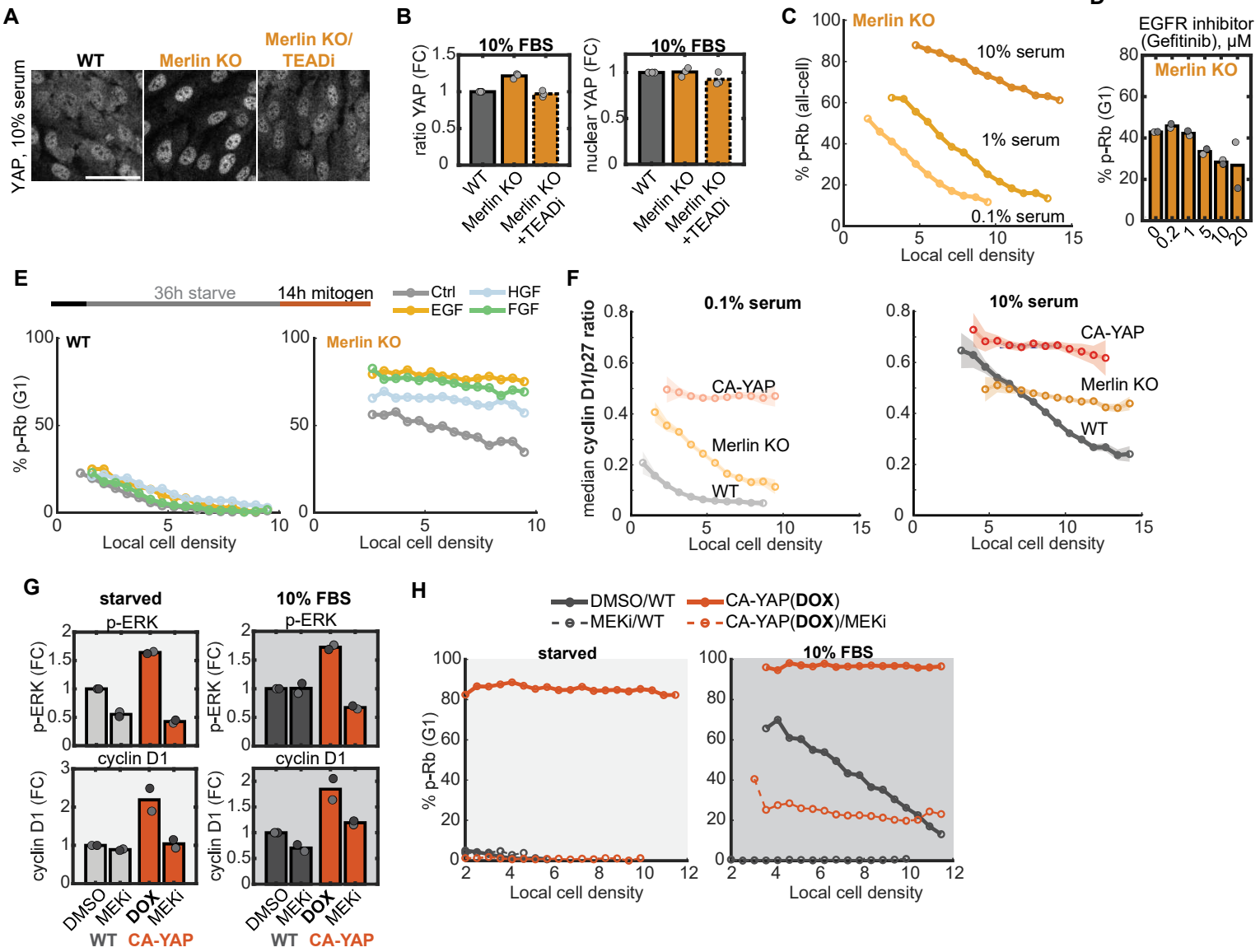
A
WT
Merlin KO
Merlin KO/ TEADi
YAP, 10% serum
B
10% FBS
ratio YAP (FC)
nuclear YAP (FC)
WT
Merlin KO
Merlin KO +TEADi
C
Merlin KO
10% serum
1% serum
0.1% serum
% p-Rb (all-cell)
Local cell density
D
EGFR inhibitor (Gefitinib), μM
Merlin KO
% p-Rb (G1)
E
36h starve
14h mitogen
Ctrl
HGF
EGF
FGF
WT
Merlin KO
% p-Rb (G1)
Local cell density
F
0.1% serum
10% serum
median cyclin D1/p27 ratio
CA-YAP
Merlin KO
WT
Local cell density
G
starved
10% FBS
p-ERK
p-ERK (FC)
cyclin D1
cyclin D1 (FC)
DMSO
MEKi
DOX
MEKi
WT
CA-YAP
H
DMSO/WT
MEKi/WT
CA-YAP(DOX)
CA-YAP(DOX)/MEKi
starved
10% FBS
% p-Rb (G1)
Local cell density

1408 **Figure S6, related to Figure 6**
1409
1410 **A)** Representative immunofluorescence images of YAP staining in WT, Merlin KO, and TEADi-
1411 treated Merlin KO (0.5 μM GNE-7883) in 10% serum. Scale bar = 50 μm.
1412 **B**) Mean fold-change in YAP ratio and nuclear YAP levels in Merlin KO treated with DMSO or
1413 TEADi relative to WT cells, as in (A). N = 3 independent experiments.
1414 **C**) Percent p-Rb per local cell density bin for Merlin KO cells maintained in titrated serum levels
1415 (gating for all cells, as in Figure 1C). N > 20,000 cells/condition, data are representative of 3
1416 independent experiments.
1417 **D**) Mean percent p-Rb for serum-starved Merlin KO cells treated with gefitinib (EGFR inhibitor)
1418 at indicated doses (μM) for 24h. N = 2 independent experiments.
1419 **E**) Top: starvation-release protocol for WT or Merlin KO cells with control (CTRL), EGF, HGF, or
1420 FGF (all 25 ng/mL). Bottom: percent p-Rb comparing WT (left) and Merlin KO (right) treated with
1421 CTRL or mitogens for 14h. N > 12,000 cells/condition, data are representative of 2 independent
1422 experiments.
1423 **F)** Median cyclin D1/p27 ratio binned by local cell density for WT (grey), Merlin KO (yellow), and
1424 CA-YAP cells (red) in 0.1% (left) or 10% serum (right). Shaded error are 95% confidence
1425 intervals, data are representative of 2 independent experiments.
1426 **G)** Mean fold-change in p-ERK (top) and cyclin D1 (bottom) for WT and DOX-induced CA-YAP
1427 cells treated as in Figure 5F in starvation (left) and 10% serum conditions (right). N = 2
1428 independent experiments, where matched colors indicate values from the same experiment.
1429 **H)** Percent p-Rb binned by local density for WT and DOX-induced CA-YAP cells starved (left) or
1430 in 10% serum (right) treated with DMSO or MEKi as in (G). Starved: n > 5,000 cells (WT), n >
1431 20,000 cells/condition (CA-YAP); 10% serum: n > 10,000 cells (WT), n > 20,000 cells/condition.
1432 Data are representative of 2 independent experiments.
1433 All binned data are G1-gated unless stated otherwise, with n > 100 cells/bin.